Title: Recruitment and organization of ESCRT-0 and ubiquitinated cargo via condensation

Sudeep Banjade*, Lu Zhu, Jeffrey Jorgensen, Sho Suzuki and Scott D. Emr*

Weill Institute for Cell and Molecular Biology, Cornell University, Ithaca, NY, USA

Department of Molecular Biology and Genetics, Cornell University, Ithaca, NY, USA

*Correspondence to: Sudeep Banjade (sudeep.banjade@cornell.edu) and Scott D. Emr (sde26@cornell.edu)

Abstract: The general mechanisms by which ESCRTs are specifically recruited to various membranes, and how ESCRT subunits are spatially organized remain central questions in cell biology. At the endosome and lysosomes, ubiquitination of membrane proteins triggers ESCRT-mediated substrate recognition and degradation. Using the yeast lysosome/vacuole, we define the principles by which substrate engagement by ESCRTs occurs at this organelle. We find that multivalent interactions between ESCRT-0 and polyubiquitin is critical for substrate recognition at yeast vacuoles, with a lower-valency requirement for cargo engagement at endosomes. Direct recruitment of ESCRT-0 induces dynamic foci on the vacuole membrane, and forms fluid condensates *in vitro* with polyubiquitin. We propose that self-assembly of early ESCRTs induces condensation, an initial step in ESCRT-assembly/nucleation at membranes. This property can be tuned specifically at various organelles by modulating the number of binding interactions.

One-Sentence Summary:

Multivalent interactions between ESCRT-0 and polyubiquitin induce condensate formation and cargo sorting at vacuoles/lysosomes.

Main Text:

Introduction

ESCRT family members consist of a group of proteins involved in controlling diverse membrane-remodeling biochemical reactions, which include multivesicular body biogenesis, HIV budding, cytokinesis and membrane repair (*1*). Many of these occur at different membrane locations in the cell (endosome, lysosome, plasma membrane and the nucleus). Although the molecules that recruit ESCRTs are mostly known, the general principles of recruitment are less well understood. The mechanisms by which ESCRT reactions are spatially controlled remain unclear. In addition, while the structure of the individual subunits of the ESCRT complexes have been in most part solved (*2–5*), the mesoscale structural organization of early ESCRTs on the membrane is unclear.

At endosomes during multivesicular body biogenesis, ubiquitinated membrane proteins (cargo) recruit ESCRT-0, which then recruits the downstream proteins ESCRTs I, II and III(*6*). Therefore, ubiquitination serves as a signal to recruit ESCRTs to the endosomal membrane. The ESCRT-I complex has two ubiquitin binding motifs, ESCRT-II has one ubiquitin binding motif (*7*), and the complex of ESCRT-0 contains at least five ubiquitin binding motifs (one VHS and two UIM motifs in the ESCRT-0 protein Vps27, and one VHS and one UIM motif in the ESCRT-0 protein Hse1, (*7*)). Therefore, the ESCRT-0 complex is a critical component of the pathway that controls cargo binding. Furthermore, ESCRT-0 has been reported to form tetramers, oligomers and clusters (*8*, *9*). *In vivo* cargo sorting occurs at hotspots (*10–12*), demonstrating cargo concentration at specific sites, although the mechanism of this organization is not understood. The presence of multivalency for ubiquitin binding in ESCRT-0, and the knowledge of the existence of poly-ubiquitinated cargo as substrate, suggest higher order assembly of these complexes, as demonstrated for various multivalent interactions (*13–15*).

In this study, to understand the principles of ESCRT and cargo organization at membranes, we set out to delineate the properties of ESCRT's initial recruitment and assembly at two similar but separate organelles in yeast endosomes and vacuoles (yeast lysosomes). We recently described the mechanism of ESCRT-mediated lysosomal protein recognition and degradation via ubiquitination of lysosomal membrane proteins (*16*). While studying the requirements of vacuolar membrane protein recognition by ESCRTs, we find that polyubiquitination is critical for efficient ESCRT

recognition at the vacuole. Higher valency of ubiquitin is more critical for cargo sorting at the vacuole than at endosomes. Polyubiquitinated proteins associate with ESCRT-0, leading to self-assembly of ESCRT-0 and cargo into dynamic condensates, which may provide a platform for nucleation of downstream ESCRT complexes.

Results

As a model cargo to study ESCRT assembly principles at endosomal and vacuolar membranes, we used the vacuolar protease carboxy-peptidase-S (CPS), which is transported to the vacuole from the Golgi via the endosomal pathway(*17*). GFP-CPS is sorted into multivesicular bodies by the action of ESCRTs and is then trafficked to the vacuolar lumen for degradation (Fig. 1A, 1C). Therefore, GFP-CPS is localized in the vacuolar lumen (Fig. 1C). In ESCRT mutants (for example in the ESCRT-0 mutants *vps27*Δ or *hse1*Δ), GFP-CPS gets stuck at aberrant endosomes (also called class-E compartments or "E-dots") (Fig. S1).

While Golgi-endosome-vacuole is one route for proteins to get to the vacuole lumen, another route to the vacuole is through the AP-3 pathway (Fig. 1A). When GFP-CPS is re-routed to the vacuole membrane by adding an AP-3 recognition site (hereafter called GFP-alp-CPS – "alp" for the "alp pathway"), the protein remains at the vacuole membrane (Fig. 1C, (*17*)). These two proteins (GFP-CPS and GFP-alp-CPS) therefore provide us with almost identical cargoes that traffic to the vacuole via two independent vesicular compartments. This design allows us to probe the properties that ESCRTs utilize for the same protein to be recognized at two different physical locations in the cell.

Our previous study indicated that ESCRTs are able to recognize ubiquitinated membrane proteins at the vacuole membrane as well, in addition to endosomes (*16*). Considering that GFP-alp-CPS is stable at the vacuole membrane and does not get internalized into the lumen, we tested if conjugating CPS with ubiquitin induces ESCRT-mediated cargo internalization. We found that when a single ubiquitin is conjugated at the N-terminus of GFP-alp-CPS, the protein now gets internalized into the lumen, in a Vps27-dependent fashion (Fig. 2A-B, Fig. S1).

Following this observation, we asked if a single ubiquitin is sufficient for complete internalization of GFP-alp-CPS on the vacuole membrane. Therefore, we used a lysine-less ubiquitin molecule (where all the seven lysines are mutated to arginines) to probe the effect of a polyubiquitin-deficient cargo. CPS normally gets ubiquitinated on K8 and K12 residues (*18*), which were mutated to Arg in this construct, and from hereon called Ub^{KR}-GFP-alp-CPS^{KR} (Fig. 2A).

We found that the internalization of this polyubiquitin-deficient cargo is inhibited and a large fraction of it remains at the vacuole membrane (Fig. 2C). Compared to the wild type ubiquitin containing lysines, the lysine-less protein does not form polyubiquitin chains (Fig. 2D). If the number of the lysine-less Ub molecules is increased making 2X-Ub^{KR} or 3X-Ub^{KR}, internalization to the lumen is rescued (Figs. 2A and 2C).

Vacuole-targeted membrane-protein cargoes are ubiquitinated through the action of E3 ligases such as Rsp5, Tul1 and Pib1 (*19*). Deletions of Rsp5-adaptors Ssh4 and Ear1, in addition to Tul1 and Pib1, had a severe defect in internalization of the vacuolar-membrane cargo Ub-GFP-alp-CPS (Fig. S2). These data provide further evidence that a higher level of ubiquitination (or polyubiquitination) is required for the vacuolar membrane protein to be recognized and sorted by ESCRTs.

Therefore, the vacuolar membrane proteome is susceptible to regulation through the ESCRT pathway and polyubiquitination of cargo is necessary for efficient sorting and degradation. To study the effect of the number of ubiquitin molecules on vacuolar protein cargo in a controlled fashion, we utilized a previously established rapamycin-dependent degradation system (*16*). In this system, the protein/cargo of interest is tagged with FKBP, and the yeast strain also contains an FRB molecule conjugated with ubiquitin. This system allowed us to control the number of ubiquitin molecules conjugated to the cargo of interest by following the kinetics of cargo sorting and degradation after addition of rapamycin, which triggers FRB-FKBP binding.

A 2X-FKBP (two FKBP molecules fused in tandem) in the presence of FRB-3XUb (three ubiquitin molecules in tandem) was effective in inducing ESCRT-mediated sorting of the vacuolar lysine-transporter Ypq1 (*20*). We modified the valency of ubiquitin bound to the cargo by mutating one of the FRB-binding sites in FKBP (called FKBP*), and by using single or triple ubiquitin

molecules fused to FRB (Figure 3A). In cargo sorting assays, we found a strong dependence on the number (valency) of ubiquitin fused to FRB (Fig.3A-D, Fig. S3A-B). The same effect is also observed when we used an orthogonal cargo Vph1, with the number of effective ubiquitin molecules controlling the level of internalization into the vacuolar lumen (Fig. S3C).

To assess whether direct recruitment of ESCRTs to the vacuolar cargo can cause degradation of the cargo, we fused the ESCRT-0 protein Vps27 to FRB. This construct is fully functional and identical to the activity of the wild-type Vps27 (Fig. S4), as it can fully complement the defect of a *vps27*Δ strain for two different cargo sorting reactions (Mup1-pHluorin and Can1 through a canavanine sensitivity assay, (*21*)).

Upon rapamycin-induced recruitment of Vps27 in this system, the modified cargo Ypq1 (fused to 2XFKBP) internalized into the vacuolar lumen and degraded over time (Fig. 3E). Interestingly, we observed formation of distinct foci of the cargo at the vacuole surface upon adding rapamycin (Fig. 3E. Fig. S5). These foci are dynamic in nature – they move over time (Movie 1, Fig. S5), and occasionally fuse with one another. Some clusters disappear over time, presumably as the cargo gets internalized into the lumen (Movie 1, Fig. S4C). The foci also tend to disappear more completely upon cycloheximide-treatment to inhibit translation and therefore new synthesis of the cargo (Fig. S4C).

When a lower valency cargo construct is used instead, where one of the FKBP sites is mutated to abrogate FRB-Vps27 binding, rapamycin-induced cargo clustering and sorting is inhibited (Fig. S6A). Importantly, this lower-valency cargo molecule is able to bind to FRB-Vps27 in a rapamycin-dependent fashion (Fig. S6B). Therefore, while ESCRT-0 is recruited, the valency of binding sites on the Ypq1 construct is critical to induce of ESCRT-mediated cargo sorting.

Our data therefore suggest that higher-valency interactions between ESCRT-0 and cargo induce clustering, sorting and degradation. To understand the basis of cargo clustering induced by ESCRT-0, we purified the ESCRT-0 proteins Vps27 and Hse1, and reconstituted the assembly reaction *in-vitro*, using His6-tagged ubiquitin as the model cargo. We fused four ubiquitin genes in tandem with one another and labeled this molecule with Cy5. Upon assembling this model ubiquitin with ESCRT-0, micron sized condensates formed on supported lipid bilayers and in

155 solution at low micromolar concentrations (Fig. 4A-C). The concentrations required for formation of condensates is lower in the nanomolar range on supported lipid bilayers and micromolar range in solution (Fig. 4A-C), implying robust formation of these assemblies. The structures also exhibit morphologies expected of liquid-like structures on membranes(Fig. 4A,(*13*)), and undergo fusion on membrane and in solution (Movies 2, 3). The clusters concentrated both ubiquitin and ESCRT-
160 0 (Hse1 labeled with Oregon Green) to approximately 10 fold (Fig. 4A). Inclusion of a single ubiquitin in the assay abrogated condensate formation, signifying the importance of ubiquitin valency in the self-assembly (Fig. 4B).

A wide range of condensate sizes, down to nanometer scale are formed (Fig. 5C) , as depicted by
165 electron microscopy (Fig. 5A). Rough edges of the condensates down to the nanometer level, and highly dense meshwork of proteins are reminiscent of network formation in such assemblies, as previously observed in other multivalent systems undergoing condensation (*15*, *22*).

These structures are dynamic since they exhibited molecular exchange ((Fig. 5B), fluorescence
170 recovery after photobleaching). Ubiquitin exchanges more rapidly than ESCRT-0, most likely because ESCRT-0 self-associates to form oligomers ((*8*, *9*) and see below for ESCRT-0 self-association). Solvent conditions are important for their formation, as condensation was favored by acidic pH (Fig. S7A). In the presence of 1X Ub and ESCRT-0 (both Vps27 and Hse1), rare condensates were observed that only weakly concentrated ubiquitin (Fig. 5C). Condensate
175 formation was possible but significantly inhibited with only Vps27 and Hse1, signifying weak self-association between the subunits of the ESCRT-0 complex (Fig. S7B), probably owing to the higher-order oligomerization and association of the intrinsically disordered regions of the complex (Fig. S6C).

180 Condensates did not form with only 4XUb, or with 4XUb and Hse1 (Fig. S7B). Without Hse1, the condensates of 4X Ub and Vps27 were smaller (Fig. S7B), as the valency of interaction is reduced. Consistent with a multivalency-mediated condensate phenomenon that exhibits a stoichiometrically undefined complex formation, the ratio of ubiquitin to ESCRT-0 varies as a function ubiquitin concentration (Fig. 5D). At the highest concentration of ubiquitin in this
185 experiment, condensate formation is inhibited as the multivalent complexes are titrated off. To test whether the condensates localize non-specific protein assemblies, we used a flurorescent His6-

tagged Snf7 protein (an ESCRT-III protein that does not have specific binding sites for ESCRT-0 or ubiquitin) in our assays. Snf7 forms bright punctate structures (most likely Snf7 polymers) outside of the clusters (Fig. S7C), suggesting that in order to localize to these ubiquitin clusters, Snf7 would require specific binding partners, a topic of further analyses in our future studies.

The aforementioned properties are hallmarks of biomolecular condensates – valency dependent cluster formation, solvent conditions controlling condensation, dense internal organization, variable stoichiometry of the complexes, domains that exclude non-specific proteins, structures that exhibit internal rearrangement of molecules and exchange with the environment (*14*). These in vitro analyses strongly indicate condensate formation as the mechanism of ESCRT-0 mediated polyubiquitin clustering.

As predicted by this model, mutations in the ubiquitin-binding motifs of Vps27 (Vps27$^{vhs\ uim\ uim}$) also inhibited condensate formation *in-vitro,* as the valency of ubiquitin-binding motifs is decreased (Fig. 6A-B). To study whether this valency-dependence of ubiquitin-binding sites has any effect in vivo on cargo sorting, we utilized the model endocytosis cargo Mup1 and its sorting assays previously described ((*23*). We made combinations of several mutations on Vps27 and Hse1, and studied the effects of these mutations on Mup1 sorting to the vacuole. The data suggested a strong valency dependence on cargo sorting, in particular suggesting a regime of low activity towards sorting with lower valency interactions and a higher activity regime with high-valency interactions (Fig. 6C-D).

Our data therefore demonstrate a critical role of multivalent interactions during cargo sorting reactions and imply clustering by condensation as the mechanism behind this role. In addition to the endosomal cargo Mup1, higher valency interactions through polyubiquitin and ESCRT-0 is also critical for cargo sorting reactions at the vacuolar membrane for several cargoes (GFP-alp-CPS, Ypq1, Vph1). Interestingly, the internalization of the lysine-less GFP-CPS molecule, (Ub^{KR}-GFP-CPS^{KR}: note without the alp signal), that traffics through the endosome, localizes to the lumen of the vacuole (Fig. 7A-C), in contrast to the vacuolar cargo (Fig. 1). Therefore, the cargo recognition and internalization of this polyubiquitin-deficient membrane protein is more severely defective at the vacuolar membrane compared to the endosomal membrane. These effects are also observed when we follow the kinetics of degradation of the vacuole-targeted cargo compared with

that of the endosome-targeted cargo. In this experiment we used a galactose inducible expression system, following the stability of the protein over time upon translation inhibition with cycloheximide (Figure 7A). Although the proteins reach the endosome/vacuole membrane (Figure 7C), the kinetics of degradation of the vacuole targeted protein is slower than that of the endosome-targeted protein (Fig. 7A-B). However, the rate of degradation can be enhanced with a 3XUb^{KR} conjugated vacuolar CPS molecule (Fig. S8). These data imply that lower valency interactions are more efficient for cargo sorting at endosomes than at vacuolar membrane.

Endosomes are sites of high density of ESCRTs (*24*). We reasoned that due to the higher density of ESCRTs at the endosomes, there is a lower requirement for multivalent interactions to recruit and condense ESCRTs at this organelle, as opposed to the vacuolar membrane. One of the lipid-species that recruit ESCRTs to the endosomal membrane is phosphatidyl-inositol-3P (PI3P). We hypothesized that an increase in PI3P density could in turn increase the density of ESCRTs, thereby reducing the requirement of higher valency interactions at the vacuolar membrane. To test this prediction, we used the PI3P phosphatase mutants *ymr1*Δ and *sjl3*Δ, which have previously been shown to increase the level of PI3P on the vacuole membrane (*25*). In the single mutants ymr1Δ and *sjl3*Δ, the single-ubiquitin conjugated vacuolar GFP-CPS (Ub^{KR}-GFP-alp-CPS^{KR}) remains mostly on the vacuole membrane (Fig. S9B). However, in the double mutant *ymr1*Δ *sjl3*Δ, the molecule is enriched in the vacuole lumen (Fig. 7D). Therefore, the defective sorting of the substrate can be rescued by the local increase in density of PI3P at the vacuolar membrane. These latter experiments suggest how multivalent intearctions, and in turn condensate formation, may function to create high-density cargo sorting sites at the vacuole membrane.

Discussion

We provide evidence for two distinct mechanisms of recruitment and organization of ESCRT complexes at two separate membrane locations: the endosomes and the vacuole (Fig. 8). Our data suggest that one of the functions of the ESCRT-0 complex, by virtue of having multiple binding sites for ubiquitin, is to facilitate cargo clustering at the membrane through biomolecular condensation. ESCRT-0 by itself has a weaker ability to self-associate and undergo condensation. When substrates are polyubiquitinated, the multivalency of ESCRT-0 enhances formation of higher-order species of the ESCRT-0/cargo complexes. Increasing the density of PI3P increases

the local concentration of ESCRT-0/ubiquitin on the membrane, thereby lowering the threshold for self-association (Fig. 4D, S10). We note that in addition to the ubiquitination of the cargo, the reported ubiquitination of Vps27 (*28*) also could enhance multivalency and ESCRT-0 self-association. The general principles behind function of ESCRTs at membranes were proposed to include - recruitment to membranes, "self-assembly", and ESCRT-III polymerization (*26*). In the context of cargo sorting reactions, condensation would provide the basis of "self-assembly", an initial event in ESCRT-mediated reactions.

Condensing cargo via early ESCRTs could provide multiple advantages in the cargo-sorting process. The physical concentration of cargo could amplify sorting of cargo, increasing the specificity for cargo recognition by ESCRTs. Concentrating downstream ESCRT complexes at a particular location and increasing the dwell time on the membrane could also provide a platform for nucleation of ESCRT-III polymerization, as observed for actin assembly pathways through upstream condensing nucleators (*27*). The rapid dynamics of ubiquitin in the condensates could allow for facile dissociation of the cargo from ESCRTs. As opposed to an ordered assembly (such as that of a clathrin-coated pit) where there likely is no internal rearrangement of the polymeric subunits, a condensate consisting of a stoichiometrically variable complex most likely requires less energy for its disassembly. This may be the reason behind the design of such clusters for spatial organization on the membrane. Furthermore, condensation of ubiquitinated cargo could feed-back to the ubiquitin-ligase machinery, allowing for enhanced ubiquitination of the cargo.

At locations in the cell where ESCRT-0 is not involved, other mechanisms of self-assembly may exist – in the case of HIV budding, the HIV Gag protein is known to form higher-order assemblies, which recruit downstream ESCRTs (*29*). Clustering and condensation of ESCRT-recruiters, therefore, could be a general property of ESCRT-related systems.

Our data provide clues for how clustering of signaling molecules can be regulated at various locations in the cell. By changing the number of binding sites for a complex on the membrane, cells may be able to quickly adjust local concentrations of enzymes and signaling adaptors. 2D surfaces and their charge properties may also play an important role in the nucleation of condensates (*30*) and also promote membrane repair and remodeling (*31*, *32*). The composition of

the membrane therefore should play a critical role in controlling the formation and function of membrane-associated biomolecular condensates.

285 **Materials and Methods**

Strains and Plasmids are listed in Table 1 (Supplementary Materials)**.**

Fluorescence Microscopy

290

For microscopy purposes of steady-state distribution of GFP-CPS (and its derivatives), Ypq1-2XFKBP-GFP and Vph1-2XFKBP-GFP, the following procedure was used. Cells were grown on YPD (yeast extract, peptdone and dextrose mixture). 1 mL of mid-log cells were centrifuged for 1-2 min at 10,000 xg and resuspended in 10-20 µL of Milli-Q water. Imaging was performed on a
295 Deltavision Elite system with an Olympus IX-71 inverted microscope using a 100X/1.4 NA oil objective. On the Softworx software, images were deconvolved using 10 iterations with the "conservative" method. Images were analyzed on Image J. Linescan images were analyzed after background subtraction and normalized to the range of 0 to 1 by dividing the intensities by the maximum intensity.

300

Live-cell imaging time-lapse microscopy was performed as follows. Chambered slides were first rinsed with Milli-Q water. 200 µL of 1 mg/mL concanavalin A was applied to the glass slide for 1 minute at room-temperature. Excess concanavalin A was removed and the slide rinsed twice with 1 mL Milli-Q water. Mid-log cells were centrifuged for 1-2 min at 10,000 xg and resuspended
305 with minimal medium. Cells were incubated on the slides for 20 minutes, then rinsed twice with 1 mL of minimal medium. Imaging was then performed on a CSU-X spinning-disk confocal microscopy system (Intelligent Imaging Innovations), coupled to a DMI 6000B microscope (Leica), 100X/1.45-NA objective and a QuantEMCCD camera. Analysis was performed on Slidebook and Image J.

310

Timelapse of the 3D droplets (Movie 3) was taken on the same CSU-X confocal microscope. Timelapse of the clusters on supported lipid bilayers (Movie 2) was taken on a Zeiss LSM 800 confocal laser scanning microscope with a 60X objective.

315 **GAL Induction and Cycloheximide Chase Assay**

GFP-CPS constructs with a GAL promoter consist of an estradiol-responsive element (*33*). For expression of the protein, cells were grown to mid-log, then 100 nM of β-estradiol was added to the medium for GAL induction. After 20 minutes, translation was stopped by adding 50 µg/mL of cycloheximide. Samples were taken (5 ODs of cells) 20 minutes after adding β-estradiol, and then
320 at subsequent times as indicated in the figures.

Rapamycin mediated FKBP-FRB interactions

Different versions of FRB-Ub, FRB-Vps27 and membrane proteins (Ypq1, Vph1) were allowed to interact through rapamycin-triggered FKBP-FRB association. All rapamycin treatment assays
325 were done similarly by adding 1 µg/mL of rapamycin to mid-log cells for different amounts of time before imaging or taking samples for immunoblots. FKBP* was made by mutating three different Rapamycin-FRB binding sites to ensure complete abrogation of FRB binding in our multivalent system. The sequences of human FKBP and FKBP* are provided below with the mutations highlighted in bold letters:

330

FKBP:

MGVQVETISPGDGRTFPKRGQTCVVHYTGMLEDGKKFDSSRDRNKPFKFMLGKQEVIR
GWEEGVAQMSVGQRAKLTISPDYAYGATGHPGIIPPHATLVFDVELLKLE

335 FKBP*:

MGVQVETISPGDGRTFPKRGQTCVVHYTGMLEDGKK**AVS**SRDANAPFKFMLGKQ**AAA**
R**GA**EEGVAQMSVGQRAKLTISPDYAYGAT**AAAAA**IPPHATLVFDVELLKLE

Immunoblots

340 Western blots were performed as follows, as described before (*34*). 5 OD equivalent of cells were collected by centrifugation at 4000 xg. After washing with 1 mL of cold H_2O, and then centrifuged again at 4000 xg, cells were precipitated with 10% TCA for >1 hr on ice. Cells were washed twice with 1 mL of acetone, resuspending pellets between washes by bath sonication. Pelleted cells were then lysed in 100 µL lysis buffer (50 mM Tris-HCl, pH 7.5, 8 M urea, 2% SDS, and 1 mM EDTA)
345 by bead beating for 10 min. 100 µL of sample buffer (150 mM Tris-Cl, pH 6.8, 8 M urea, 10%

SDS, 24% glycerol, 10% v/v βME, and bromophenol blue) was then added to the sample and vortexed for 10 min. After centrifugation for 6 min at 21,000 xg, supernatant was loaded on an SDS-PAGE gel and transferred onto a nitrocellulose membrane. Imaging of the western blots was performed using an Odyssey CLx imaging system and analyzed using the Image Studio Lite 4.0.21 software (LI-COR Biosciences). Fractional degradation of the GFP tagged proteins were quantified by dividing the intensity of the GFP band from the sum of the intensities of the full-length and the cleaved-GFP bands.

Denaturation IP for Ubiquitination Assay

Ubiquitination of the CPS constructs were performed in a strain background of *doa4*Δ *pep4*Δ *prb1*Δ. CPS constructs were integrated into this strain and ubiquitin was overexpressed using a myc-Ub construct under the control of a copper promoter. The copper promoter was induced by adding 100 µM $CuSO_4$ for 4 hours to mid-log cells. 100 OD equivalent of cells were harvested and washed with Milli-Q water. Cells were resuspended in urea containing buffer (50 mM Tris-HCl pH 8.0, 1% SDS, 8 M urea, 20 mM NEM, 1X Roche protease inhibitor without EDTA). Cells were lysed with zirconia beads from Biospec (about 500 □L of bead volume), by vortexing twice for 30 s at 4° C. Cells were then chilled on ice for 10 minutes. An equivalent volume of a high-salt containing buffer (50 mM Tris-HCl pH 8.0, 500 mM NaCl, 10% glycerol, 20 mM NEM, 0.2% Triton X 100) was added to the lysate and chilled again on ice for 10 min. After centrifugation for 10 min at 16,00 xg, supernatant was incubated with anti-GFP beads (at a volume ratio of 1:50 beads:solution). This mixture was rotated for 2 hours at 4° C. Beads were washed with wash buffer (50 mM Tris-HCl pH 8.0, 250 mM NaCl, 0.5% SDS, 4 M urea, 20 mM NEM, 5% glycerol), 3 times equaling an 8000-fold dilution. Elution was performed by boiling the beads at 98° C for 3 minutes in 100 µL of sample buffer (150 mM Tris-Cl, pH 6.8, 8 M urea, 10% SDS, 24% glycerol, 10% v/v βME, and bromophenol blue). Samples were then blotted for GFP and ubiquitin.

Canavanine Assay and Mup1-Sorting Assay

These assays were performed exactly as described before (*21*, *34*, *35*). Briefy, canavanine spot plates were performed on synthetic media with canavanine at various concentrations and imaged after 3-5 days. Mup1 sorting assay was performed on Mup1-pHluorin integrated cells after addition of 20 µg/mL at various time points. Fluorescence measurements were done on a BD Accuri C6 flow cytometer.

Formation of Lipid Monolayers, Liposomes and Supported Lipid Bilayers

Monolayers were formed as previously described(*21*, *34*, *35*). Supported lipid bilayers were formed as follows, following previous protocols (*5*).

To form the supported bilayers, liposomes were first created by extrusion. Lipid mixtures of 2% Ni^{2+}-NTA DOGS and 98% POPC were created in chloroform. These lipid mixtures were allowed to evaporate overnight in a desiccator. The dried mixture was hydrated in 25 mM Hepes pH 7.5, 150 mM NaCl for ~ half an hour at room temperature with vortexing every 5 min. These multilamellar vesicles were used to create small unilamellar vesicles (SUVs) by extrusion through a 100 nm extrusion filter (Avanti).

To make supported lipid bilayers, 96-well plate glass bottomed plates (Cellvis) were used. Plates were cleaned by treating with 5% Hellmanex solution and incubating at 42 ° C for 30 minutes. After thorough cleaning with Milli Q water, the plates were then treated with 6 M NaOH at room-temperature for 2 hours. The plates were again thoroughly washed with Milli Q water. To make supported bilayers, the liposome mixture was warmed to 37 ° C and then applied to the cleaned glass-bottomed wells. After incubating at room-temperature for 10 minutes, unabsorbed vesicles were washed with BSA buffer (25 mM Hepes pH 7.5, 150 mM NaCl, 0.1% BSA). The plates were allowed to sit in this buffer for 30 minutes. Proteins were then added to this buffer and incubated for various times as indicated in the text for analysis of assembly on the membrane surface. Imaging was performed with either Deltavision widefield or a Leica Confocal microscope.

Protein Purification:

All proteins were expressed in the Rosetta strain. Lysis was performed by sonication on ice. Lysed cells were cleared by centrifugation at 26,000 x g for 40 minutes at 4 ˚C. Affinity purification of his-tagged proteins were performed using the Talon cobalt beads .

<u>Ubiquitin:</u>

Ubiquitin constructs had an N-terminal His6-SUMO tag followed by a His6 tag and an N-terminal cysteine for maleimide-dye conjugation. 1X ubiquitin was expressed with 0.25 mM IPTG at 37 ˚C for 4 hours, and 4X Ub was expressed with 0.5 mM IPTG at 18 ˚C overnight. After affinity

purification with cobalt beads, and cleavage of His6-SUMO on beads, 4X-Ub was passed through a Hi-Trap S-Sepharose cation exchange column, and the flow-through collected. 1X-Ub was purified with cobalt beads and H6-Sumo cleaved on beads. Subsequently, these ubiquitin proteins were treated with 1 mM fresh DTT, and then ran though SD200 in buffer lacking reducing agent for labeling. Proteins were concentrated and incubated with Cy3 or Cy5-maleimide (Lumiprobe) at 5-fold excess and room-temperature to label the proteins. Excess dye was removed by running through a Hi-Trap Q column and dialysis. Unlabeled proteins were similarly flash-frozen right after the SD200 step.

ESCRT-0:

Vps27 and Hse1 constructs for expression were made in the pET28a vector containing an N-terminal His6 and SUMO tags and a C-terminal S-tag. Proteins were expressed at 18˚C overnight with 1 mM IPTG. After Co^{2+} column, the SUMO tag was cleaved on beads by the protease ULP overnight at 4 ˚C. The cleaved protein was then applied to an S-column. The flow-through from this step was then concentrated and ran through an SD200 column. A substantial fraction of the Vps27 protein comes out in the void volume, which is not used in the study as the nature of this fraction of protein is not clear, but it is possible that this population also reflects a fraction that is self-assembling. We collect the fraction that enters the column for our studies. Hse1-oregon green and Vps27-oregon green were made using the same labeling protocol as ubiquitin. In this case, the endogeneous cysteines on Hse1 were used for labeling purposes. Our experiments contain 10% fluorescently labeled.

Initial experiments with ESCRT-0 complex was also purified from *S. cerevisiae* using GAL promoters. In this approach, Hse1 was tagged with GFP at the N-terminus, followed by a Prescission cleavage site. GFP-prescission-Hse1 under a GAL promoter was expressed together with Vps27 (also under GAL promoter) in the same vector. This plasmid was integrated into a strain consisting of a Gal4-ER-VP16 system, whose expression can be induced by applying β-estradiol. This strain was grown at 30 deg C until mid-log, and induced with 100 nM β-estradiol until saturation. Cells were collected and lysed using a freezer mill. GFP-prescission-Hse1 was affinity-purified using a home-made GFP-nanobody agarose column. The Hse1-Vps27 complex was cleaved off by using Prescission protease on beads at 4 deg C for ~16 hours. Cleaved protein was concentrated and purified further using an SD200 column (GE), in 25 mM Hepes pH 7.5, 150

mM NaCl and 10% glycerol. Protein was flash-frozen in liquid nitrogen and stored at -80 deg C. This complex was used for the electron microscopy experiments.

FRAP (Fluorescence Recovery after Photobleaching)

4XUb-Cy5 and Hse1-Oregon Green FRAP were performed on a on a CSU-X spinning-disk confocal microscopy system (Intelligent Imaging Innovations), coupled to a DMI 6000B microscope (Leica), 100X/1.45-NA objective and a QuantEMCCD camera. Analysis was performed on Slidebook and Image J. Three whole droplets were bleached with either the 647 or the 488 laser. Fluorescence values of unbleached droplets were taken to correct for photobleaching while imaging.

Electron Microscopy

On the monolayer-grids, proteins were incubated for 1 hour. Grids were stained with 2% ammonium molybdate. Electron microscopy of the monolayers associating proteins was performed on an FEI Morgagni 268 TEM.

References:

1. M. Vietri, M. Radulovic, H. Stenmark, The many functions of ESCRTs. *Nat. Rev. Mol. Cell Biol.* **21**, 25–42 (2020).

2. M. S. Kostelansky, C. Schluter, Y. Y. C. Tam, S. Lee, R. Ghirlando, B. Beach, E. Conibear, J. H. Hurley, Molecular architecture and functional model of the complete yeast ESCRT-I heterotetramer. *Cell*. **129**, 485–498 (2007).

3. J. McCullough, A. K. Clippinger, N. Talledge, M. L. Skowyra, M. G. Saunders, T. V. Naismith, L. A. Colf, P. Afonine, C. Arthur, W. I. Sundquist, P. I. Hanson, A. Frost, Structure and membrane remodeling activity of ESCRT-III helical polymers. *Science*. **350**, 1548–1551 (2015).

4. S. Tang, W. M. Henne, P. P. Borbat, N. J. Buchkovich, J. H. Freed, Y. Mao, J. C. Fromme, S. D. Emr, Structural basis for activation, assembly and membrane binding of ESCRT-III Snf7 filaments. *Elife*. **4** (2015), doi:10.7554/eLife.12548.

5. T. G. Flower, Y. Takahashi, A. Hudait, K. Rose, N. Tjahjono, A. J. Pak, A. L. Yokom, X. Liang, H.-G. Wang, F. Bouamr, G. A. Voth, J. H. Hurley, A helical assembly of human ESCRT-I scaffolds reverse-topology membrane scission. *Nat Struct Mol Biol*. **27**, 570–580 (2020).

6. D. J. Katzmann, C. J. Stefan, M. Babst, S. D. Emr, Vps27 recruits ESCRT machinery to endosomes during MVB sorting. *J Cell Biol*. **162**, 413–423 (2003).

7. J. H. Hurley, S. D. Emr, The ESCRT complexes: structure and mechanism of a membrane-trafficking network. *Annu Rev Biophys Biomol Struct*. **35**, 277–298 (2006).

8. T. Wollert, J. H. Hurley, Molecular mechanism of multivesicular body biogenesis by ESCRT complexes. *Nature*. **464**, 864–869 (2010).

9. J. R. Mayers, I. Fyfe, A. L. Schuh, E. R. Chapman, J. M. Edwardson, A. Audhya, ESCRT-0 assembles as a heterotetrameric complex on membranes and binds multiple ubiquitinylated cargoes simultaneously. *J Biol Chem*. **286**, 9636–9645 (2011).

10. E. B. Frankel, A. Audhya, ESCRT-dependent cargo sorting at multivesicular endosomes. *Semin Cell Dev Biol*. **74**, 4–10 (2018).

11. M. A. Y. Adell, S. M. Migliano, S. Upadhyayula, Y. S. Bykov, S. Sprenger, M. Pakdel, G. F. Vogel, G. Jih, W. Skillern, R. Behrouzi, M. Babst, O. Schmidt, M. W. Hess, J. A. Briggs, T. Kirchhausen, D. Teis, Recruitment dynamics of ESCRT-III and Vps4 to endosomes and implications for reverse membrane budding. *Elife*. **6** (2017), doi:10.7554/eLife.31652.

12. C. MacDonald, J. A. Payne, M. Aboian, W. Smith, D. J. Katzmann, R. C. Piper, A family of tetraspans organizes cargo for sorting into multivesicular bodies. *Dev Cell*. **33**, 328–342 (2015).

13. S. Banjade, M. K. Rosen, Phase transitions of multivalent proteins can promote clustering of membrane receptors. *Elife*. **3** (2014), doi:10.7554/eLife.04123.

14. S. F. Banani, H. O. Lee, A. A. Hyman, M. K. Rosen, Biomolecular condensates: organizers of cellular biochemistry. *Nat Rev Mol Cell Biol*. **18**, 285–298 (2017).

15. P. Li, S. Banjade, H.-C. Cheng, S. Kim, B. Chen, L. Guo, M. Llaguno, J. V. Hollingsworth, D. S. King, S. F. Banani, P. S. Russo, Q.-X. Jiang, B. T. Nixon, M. K. Rosen, Phase transitions in the assembly of multivalent signalling proteins. *Nature*. **483**, 336–340 (2012).

16. L. Zhu, J. R. Jorgensen, M. Li, Y.-S. Chuang, S. D. Emr, ESCRTs function directly on the lysosome membrane to downregulate ubiquitinated lysosomal membrane proteins. *Elife*. **6** (2017), doi:10.7554/eLife.26403.

17. G. Odorizzi, M. Babst, S. D. Emr, Fab1p PtdIns(3)P 5-kinase function essential for protein sorting in the multivesicular body. *Cell*. **95**, 847–858 (1998).

18. D. J. Katzmann, M. Babst, S. D. Emr, Ubiquitin-dependent sorting into the multivesicular body pathway requires the function of a conserved endosomal protein sorting complex, ESCRT-I. *Cell*. **106**, 145–155 (2001).

19. X. Yang, W. Zhang, X. Wen, P. J. Bulinski, D. A. Chomchai, F. M. Arines, Y.-Y. Liu, S. Sprenger, D. Teis, D. J. Klionsky, M. Li, TORC1 regulates vacuole membrane composition

through ubiquitin- and ESCRT-dependent microautophagy. *J Cell Biol*. **219**, e201902127 (2020).

20. M. Li, Y. Rong, Y.-S. Chuang, D. Peng, S. D. Emr, Ubiquitin-dependent lysosomal membrane protein sorting and degradation. *Mol Cell*. **57**, 467–478 (2015).

21. S. Banjade, S. Tang, S. D. Emr, Genetic and Biochemical Analyses of Yeast ESCRT. *Methods Mol. Biol.* **1998**, 105–116 (2019).

22. T. M. Franzmann, M. Jahnel, A. Pozniakovsky, J. Mahamid, A. S. Holehouse, E. Nüske, D. Richter, W. Baumeister, S. W. Grill, R. V. Pappu, A. A. Hyman, S. Alberti, Phase separation of a yeast prion protein promotes cellular fitness. *Science*. **359** (2018), doi:10.1126/science.aao5654.

23. S. Banjade, Y. H. Shah, S. Tang, S. D. Emr, Design principles of the ESCRT-III Vps24-Vps2 module. *eLife*. **10**, e67709 (2021).

24. D. Teis, S. Saksena, B. L. Judson, S. D. Emr, ESCRT-II coordinates the assembly of ESCRT-III filaments for cargo sorting and multivesicular body vesicle formation. *EMBO J.* **29**, 871–883 (2010).

25. W. R. Parrish, C. J. Stefan, S. D. Emr, Essential role for the myotubularin-related phosphatase Ymr1p and the synaptojanin-like phosphatases Sjl2p and Sjl3p in regulation of phosphatidylinositol 3-phosphate in yeast. *Mol Biol Cell*. **15**, 3567–3579 (2004).

26. J. Votteler, C. Ogohara, S. Yi, Y. Hsia, U. Nattermann, D. M. Belnap, N. P. King, W. I. Sundquist, Designed proteins induce the formation of nanocage-containing extracellular vesicles. *Nature*. **540**, 292–295 (2016).

27. L. B. Case, X. Zhang, J. A. Ditlev, M. K. Rosen, Stoichiometry controls activity of phase-separated clusters of actin signaling proteins. *Science*. **363**, 1093–1097 (2019).

28. D. K. Stringer, R. C. Piper, A single ubiquitin is sufficient for cargo protein entry into MVBs in the absence of ESCRT ubiquitination. *J Cell Biol*. **192**, 229–242 (2011).

29. L.-A. Carlson, J. A. G. Briggs, B. Glass, J. D. Riches, M. N. Simon, M. C. Johnson, B. Müller, K. Grünewald, H.-G. Kräusslich, Three-Dimensional Analysis of Budding Sites and Released Virus Suggests a Revised Model for HIV-1 Morphogenesis. *Cell Host & Microbe*. **4**, 592–599 (2008).

30. W. T. Snead, A. S. Gladfelter, The Control Centers of Biomolecular Phase Separation: How Membrane Surfaces, PTMs, and Active Processes Regulate Condensation. *Mol Cell*. **76**, 295–305 (2019).

31. A. von Appen, D. LaJoie, I. E. Johnson, M. J. Trnka, S. M. Pick, A. L. Burlingame, K. S. Ullman, A. Frost, LEM2 phase separation promotes ESCRT-mediated nuclear envelope reformation. *Nature*. **582**, 115–118 (2020).

32. F. Yuan, H. Alimohamadi, B. Bakka, A. N. Trementozzi, K. J. Day, N. L. Fawzi, P. Rangamani, J. C. Stachowiak, Membrane bending by protein phase separation. *Proc Natl Acad Sci U S A*. **118**, e2017435118 (2021).

33. R. S. McIsaac, S. J. Silverman, M. N. McClean, P. A. Gibney, J. Macinskas, M. J. Hickman, A. A. Petti, D. Botstein, Fast-acting and nearly gratuitous induction of gene expression and protein depletion in Saccharomyces cerevisiae. *Mol Biol Cell*. **22**, 4447–4459 (2011).

34. S. Banjade, S. Tang, Y. H. Shah, S. D. Emr, Electrostatic lateral interactions drive ESCRT-III heteropolymer assembly. *Elife*. **8** (2019), doi:10.7554/eLife.46207.

35. W. M. Henne, N. J. Buchkovich, Y. Zhao, S. D. Emr, The endosomal sorting complex ESCRT-II mediates the assembly and architecture of ESCRT-III helices. *Cell*. **151**, 356–371 (2012).

36. X. Su, J. A. Ditlev, M. K. Rosen, R. D. Vale, Reconstitution of TCR signaling using supported lipid bilayers. *Methods Mol Biol*. **1584**, 65–76 (2017).

Acknowledgments

We thank all the past and current members of the Emr lab for valuable discussions, Yuxin Mao for some initial ubiquitin constructs, and Jeremy Baskin and Brittany White, Anthony Bretscher and Rob Gringas for imaging resource. Sudeep Banjade was an HHMI fellow of the Damon Runyon Cancer Research Foundation. This work was also supported by a Cornell University Grant to Scott D Emr.

Funding

Damon Runyon Cancer Research Fellowship (through HHMI): DRG-2273-16
Cornell University Grant CU3704 to Scott D. Emr

Author Contributions

Conceptualization: SB

Methodology: SB, LZ, JJ, SS

Investigation: SB

Funding acquisition: SB, SDE

Supervision: SDE

Writing – original draft: SB

Writing – review & editing: SB, SS, SDE

Competing interests: Authors declare no competing interests.

Data and materials availability: All data are available in the main text or the supplementary materials. Strains and plasmids can be shared upon request.

585

Supplementary Materials

Figs. S1 to S10

Table S1

590

Figure 1

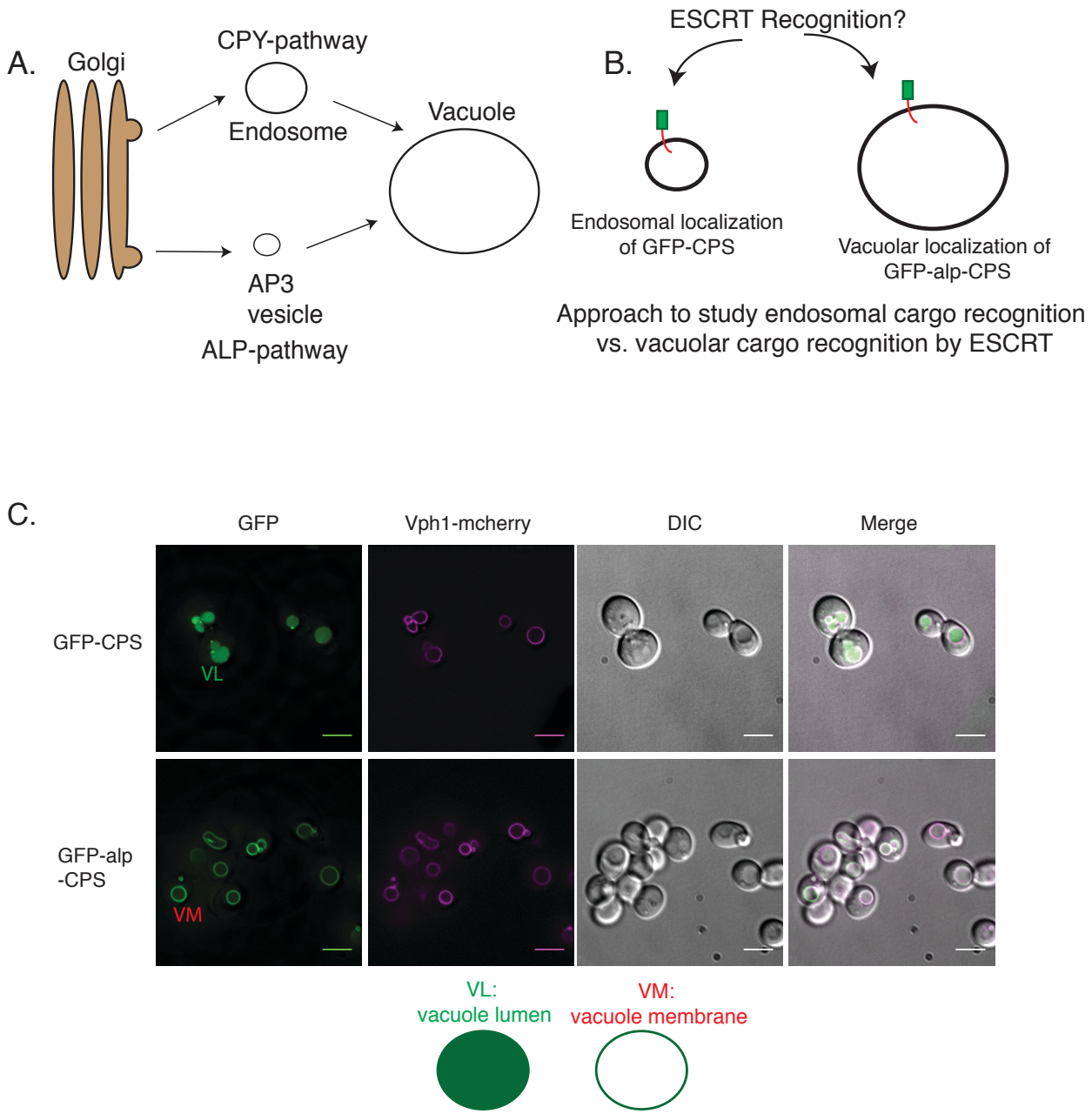

Fig. 1. Engineered CPS routed through the AP3 pathway localizes to the vacuolar membrane. A) Model of carboxy peptidase S (CPS) and ALP trafficking to the vacuole. CPS traffics through the "CPY-pathway"/endosome where MVBs are formed by ESCRTs. The ALP-pathway forms separate vesicles that traffics proteins like the alkaline phosphatase to the vacuole. **B)** Model for the localization of GFP-CPS and GFP-alp-CPS at two sites where ESCRTs can function, providing a tool to study the same cargo at two

membrane locations in the cell. **C**) GFP-CPS or GFP-alp-CPS in wild-type strains expressing Vph1-mcherry. Vph1 is a vacuolar membrane protein. Scale bars are 5 µm. Model figure below describes localization pattern of vacuolar luminal (VL) or vacuolar membrane (VM) signals.

Figure 2

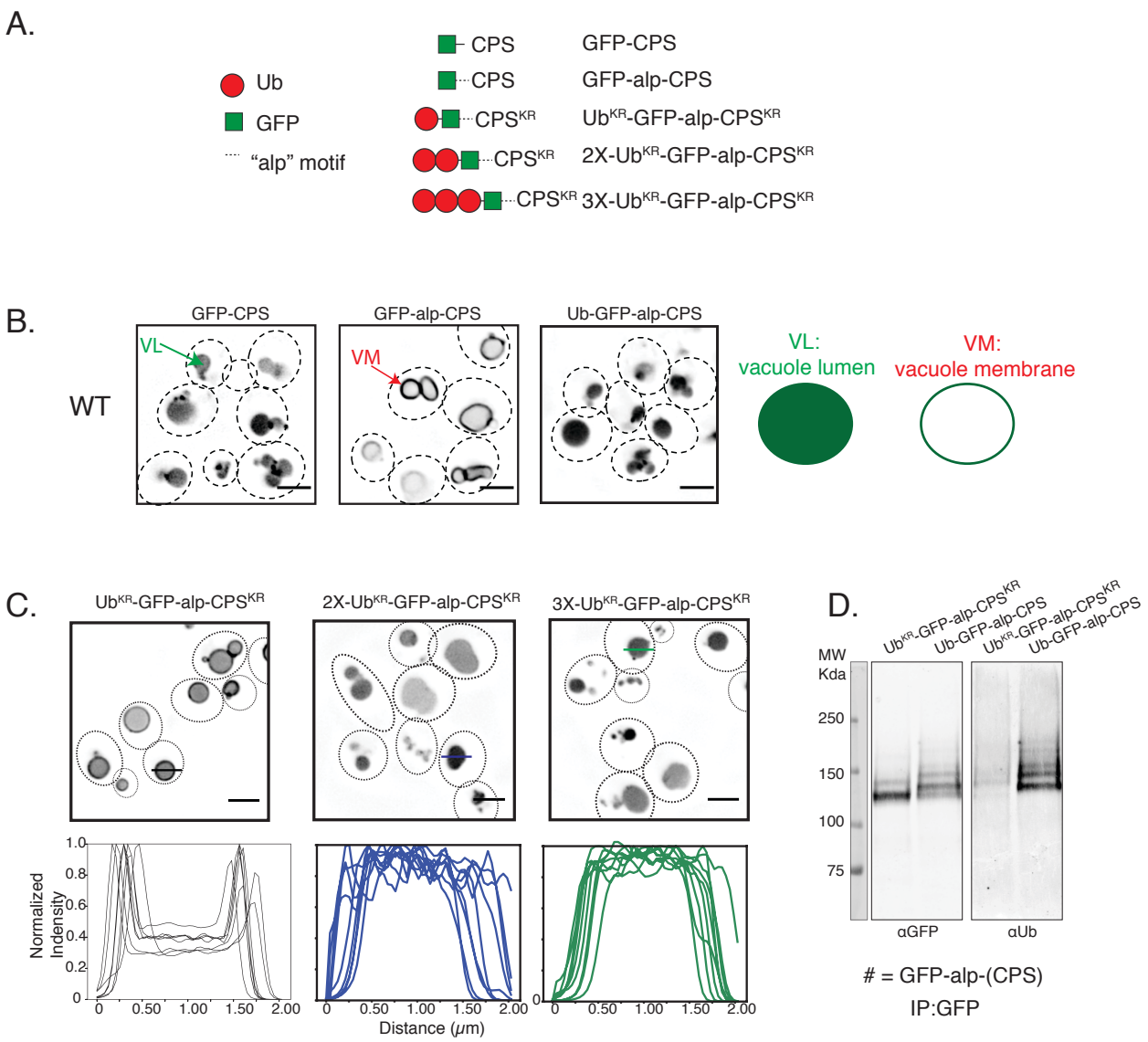

Fig. 2. Polyubiquitination is required for efficient ESCRT-dependent cargo sorting at the vacuole.

A) Different CPS constructs used in this experiment. **B)**Localization of the CPS constructs as listed on top of the figures in a WT strain. The dotted lines represent outlines of yeast

cells as imaged through the DIC channel. For simplicity the DIC channel is not shown but
610 some images with the DIC channel are shown in the supplements (Fig S1). Note that VL denotes vacuolar lumen, VM denotes vacuole membrane. Right: A model of different variants of GFP-CPS localizing in the vacuolar lumen(VL) or vacuolar membrane (VM). Scale bars are 2 µm long. **C)** Localization of the GFP-CPS constructs as denoted in the figure. UB^{KR} has all the lysines mutated to Arg. Intensity profiles on the bottom represent
615 line scan across the vacuoles. Representative lines are shown across three vacuoles (black, blue and green lines) in the microscopy images. Scale bars are 2 µm long. **D)** Immunoblots of UB^{KR}-GFP-alp-CPS^{KR} (lysine-less substrate) and Ub-GFP-alp-CPS after performing immunoprecipitation with anti-GFP. These experiments were performed in a *doa4*Δ *pep4*Δ *prb1*Δ background strain.

Figure 3

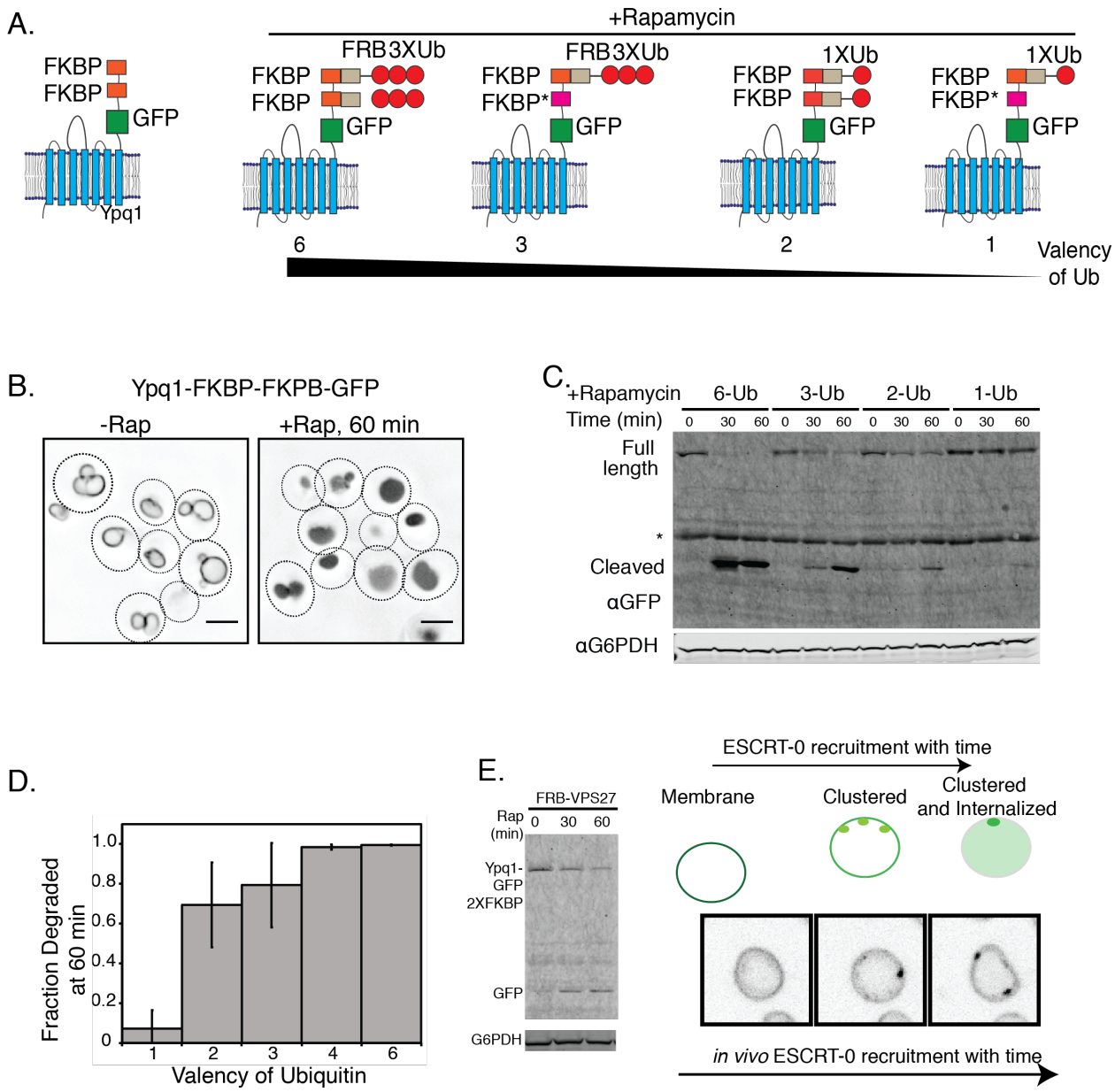

620

Figure 3. Multivalent interactions drive cargo clustering and sorting at the vacuole. **A)** Models of Ypq1 the FRB constructs used in B-D. FKBP* contains mutations on the FRB-binding sites. **B)** Localization of Yqp1 constructs with and without rapamycin addition for 60 minutes. **C)** Immunoblots for GFP after addition of Rapamycin for the

625 indicated times. The free GFP band appears and increases in intensity as the full-length protein gets internalizes into the vacuole lumen. **D)** Quantification of the fraction GFP degraded into the vacuole lumen, at 60 minutes, from the data in **C)**. **E)** Recruiting FRB-Vps27 onto the vacuolar cargo Ypq1-GFP-2XFKBP induces degradation of the cargo. **E)**

Recruitment of FRB-Vps27 onto the vacuole via binding to Ypq1-GFP-2XFKBP also induces formation of foci on the surface of the vacuole.

Figure 4

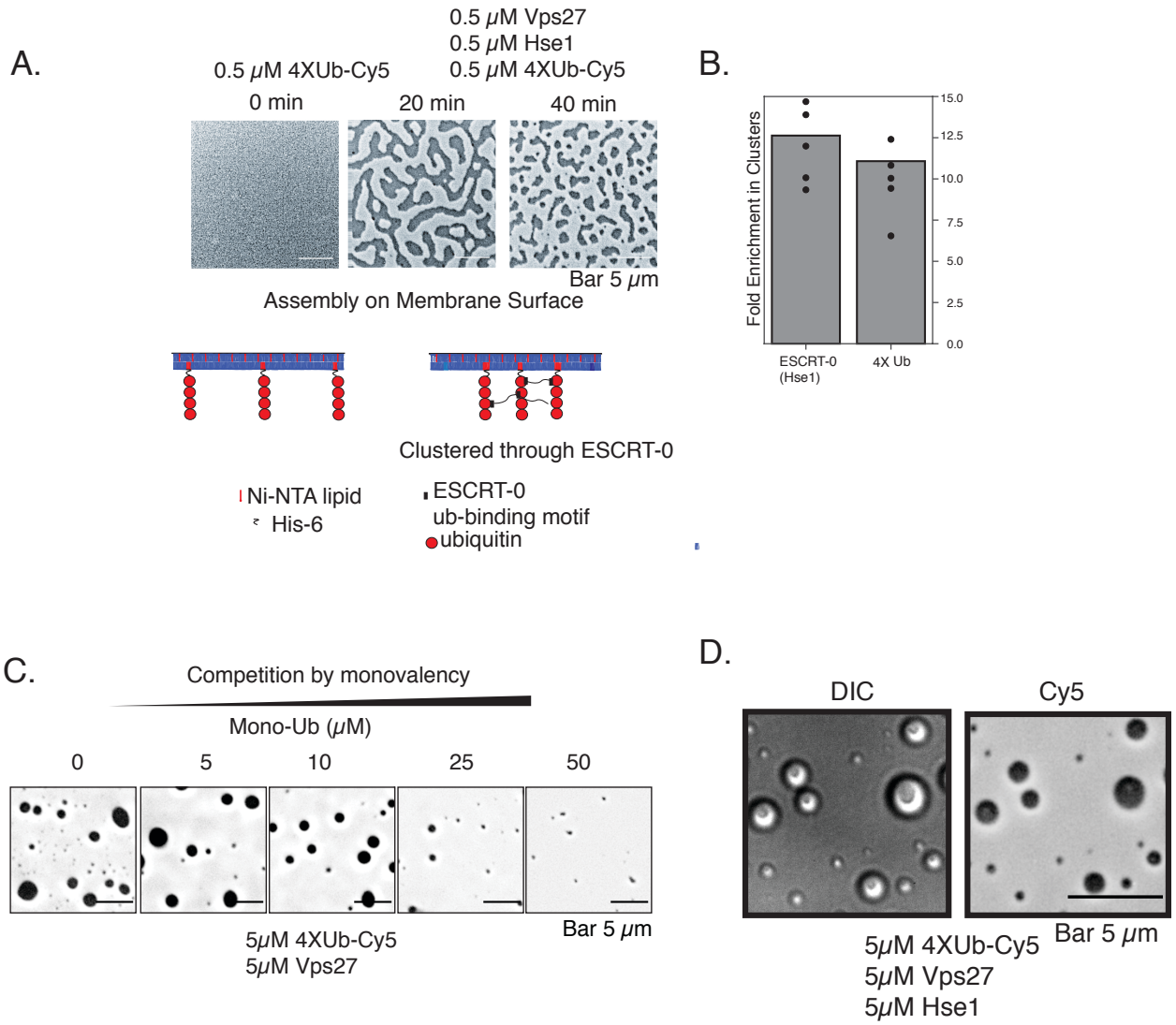

Figure 4. ESCRT-0 and polyubiquitin coassemble into condensates. A) Assembly of Vps27-Hse1 and Cy5-labeled His6-4XUb on supported lipid bilayers consisting of 2% Ni-NTA-PE. Bottom model-figure shows how 4X-Ub is associated with lipid bilayers. Model of ubiquitin binding motifs represent only a fraction of the ESCRT-0 complex. **B)** Quantification of the density of 4X-Ub-Cy5 and Hse1-Oregon Green in the membrane clusters relative to the surrounding membrane. The bars denote average of the data from five clusters (denoted by the data points)**. C)** Competition experiment of the condensates

640 with the inclusion of mono-ubiquitin at the mentioned concentrations. Protein components were combined and fluorescence of Cy5 imaged after 2 hours at room temperature. Experiments were performed in 25 mM Bis-Tris pH 6.5, 150 mM NaCl. **D)** Recombinant Vps27 and Hse1 were incubated with 4X-Ub-Cy5 and imaged after 2 hours at room temperature, showing DIC image on the left and fluorescence (of Cy5) on the right.
645 Experiments were performed in 25 mM Bis-Tris pH 6.5, 150 mM NaCl.

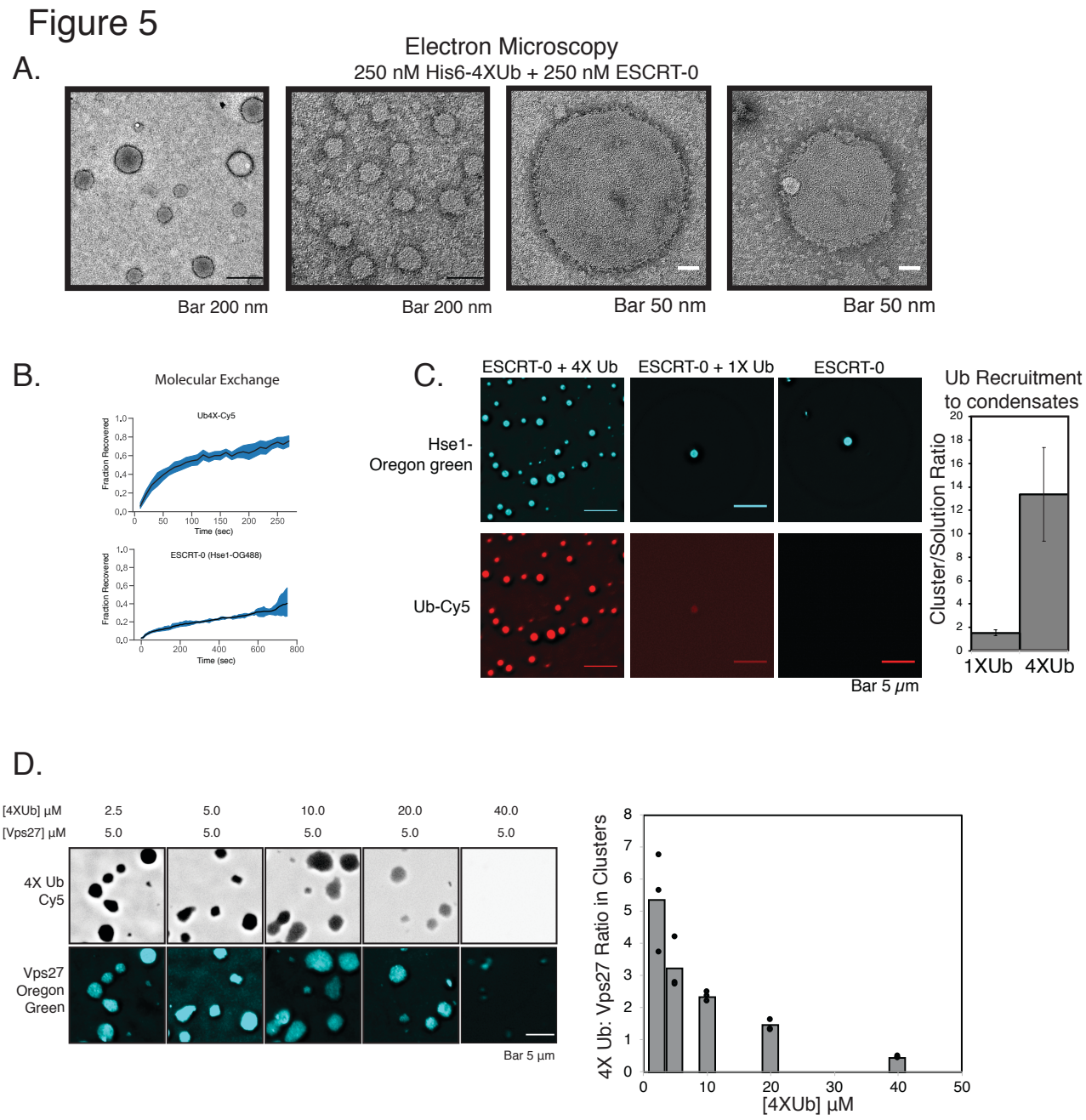

Figure 5. Multivalent interactions drive ESCRT-0 and ubiquitin condensation. A) Electron microscopy images of the ESCRT-0 complex (Vps27/Hse1) with His6-4X-Ub. The structures form variable sizes distributions and are spherical in nature. Electron microscopy was performed at 25 mM Hepes pH 7.5, 150 mM NaCl. **B)** Fluorescence recovery after photobleaching (FRAP) of 4XUb-Cy5 and Hse1-Oregon Green. Three whole droplets were bleached to obtain the normalized fluorescence recovery curves. **C)** Purified Vps27 and Hse1 were incubated with 4X-Ub and imaged after 2 hours at room

temperature. 4X-Ub contains a His6 tag at the N-terminus and also a cysteine that has been labeled with a Cy5 dye for visualization. Hse1 was labeled with Oregon-green maleimide. Right figure is a quantification of the level of mono-ubiquitin-Cy5 or tetraubiquitin-Cy5 recruitment in droplets made from respective proteins. **D)** Droplet formation at different concentrations of 4X-Ubiquitin-Cy5 (50 nM labeled) with a fixed concentration of Vps27 (1% labeled). Figure on the right represents ratios of 4X-Ubiquitin to Vps27 at different concentrations of 4X Ubiquitin.

Figure 6

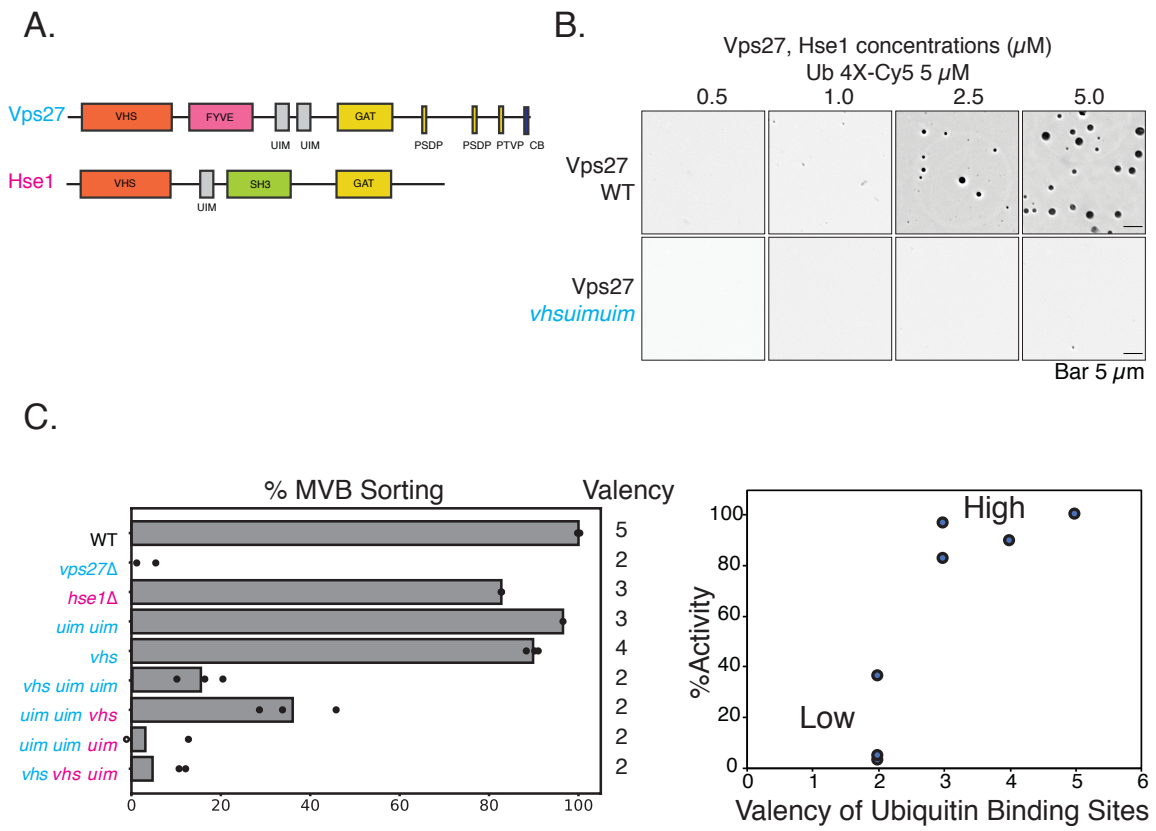

Figure 6. ESCRT-0 multivalency drive condensation and cargo sorting reactions. A) Domain organization of the ESCRT-0 proteins Vps27 and Hse1. Vps27 contains three ubiquitin binding domains (a VHS and two UIMs), while Hse1 contains two (a VHS and a UIM motif). **B)** Condensate formation with WT Vps27 or the Vps27 *vhsuimuim* mutant, in the presence of Hse1 and 4XUb-Cy5. Experiments were performed in 25 mM Bis-tris pH6.5, 150 mM NaCl. The mutant Vps27 contains mutations in the VHS domain and

mutations in the UIM motifs that abrogate ubiquitin binding. **C)** Mup1-pHluorin sorting assay through flow cytometry with different ESCRT-0 mutants. Mutations were made in the ESCRT-0 components Vps27 and Hse1 at their VHS and UIM motifs. Cyan italics represent mutations in Vps27, and the magenta italics represent mutations in Hse1. Numbers on the right of the panel represent the number of ubiquitin binding sites present in the ESCRT-0 complex in the various mutants. Dots in the bars represent independent experiments, while the bars represent average sorting from three independent experiments. Right: Sorting activity (as obtained from F) for Mup1-phluorin sorting as a function of ubiquitin valency in ESCRT-0.

Figure 7

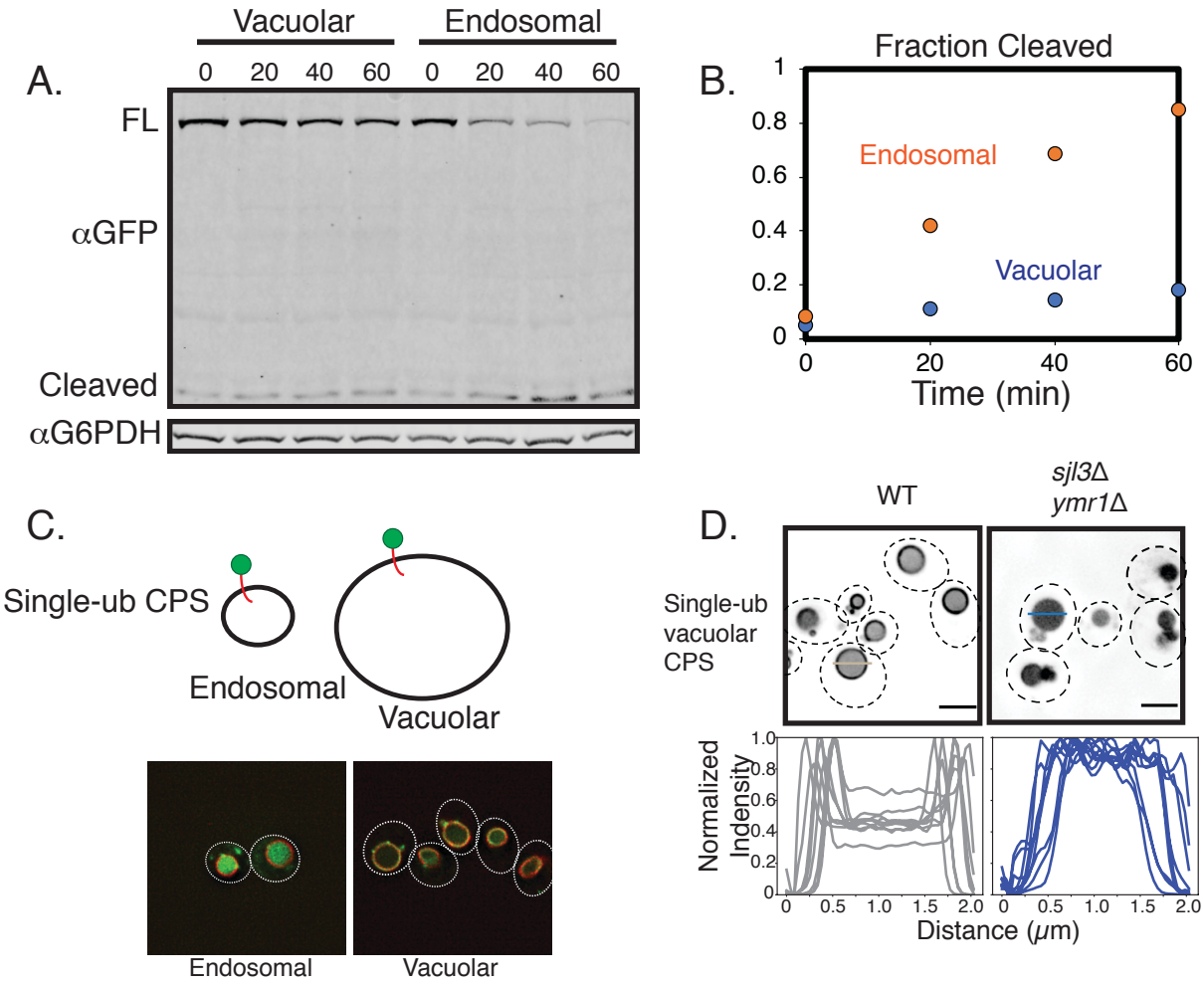

Figure 7. Differential dependence of valency on cargo sorting of endosomal and vacuolar cargoes. A) Kinetics of the degradation of UB^{KR}-GFP-CPS^{KR} (endosomal) and UB^{KR}-GFP-alp-CPS^{KR} (vacuolar) proteins upon induction of expression for 20 minutes and further inhibition of translation with cycloheximide addition. The zero timepoint represents 20 minutes of GAL induction with no cyloheximide. **B)** Quantification of the fraction of GFP cleaved of the data from **A). C)** Localization of the UB^{KR}-GFP-CPS^{KR} (endosomal) and the UB^{KR}-GFP-alp-CPS^{KR} (vacuolar) constructs after inducing the expression for 20 minutes through the GAL promoter and then stopping translation through cycloheximide addition for 30 minutes. **D)** Localization of the indicated UB^{KR}-GFP-alp-CPS^{KR} (vacuolar cargo) in the phosphatase mutant strains in the phosphatidyl-inositol-3P phosphatase mutant *ymr1*Δ *sjl3*Δ. Intensity profiles on the bottom represent line scan across the vacuoles. Representative lines are shown across two vacuoles (gray and blue lines) in the microscopy images. Scale bars are 2 µm long.

Figure 8

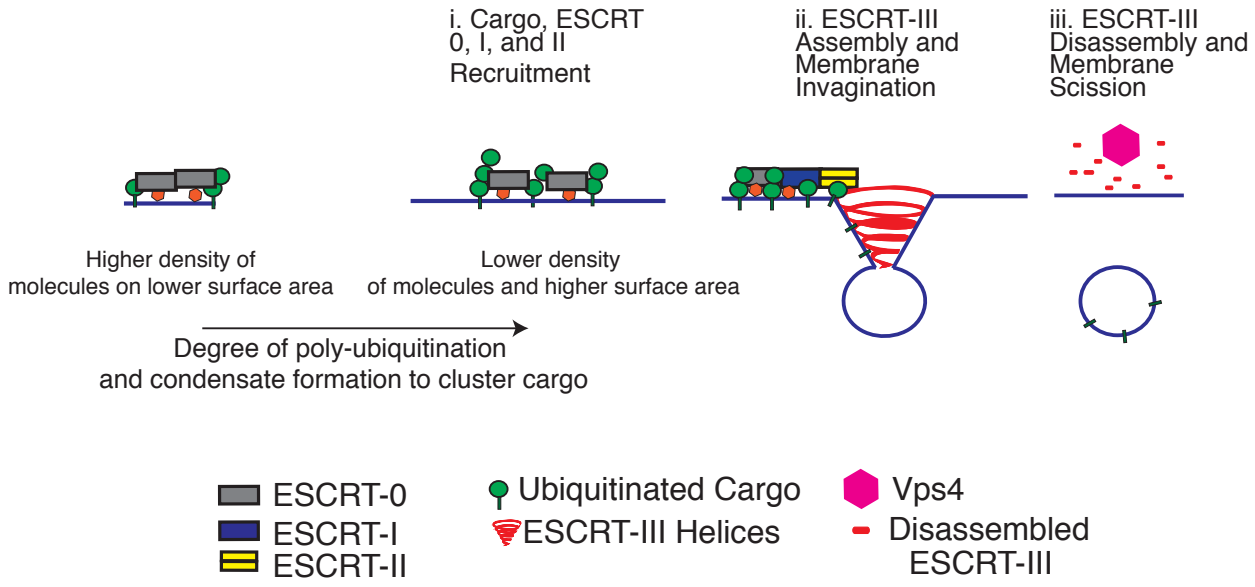

Figure 8. ESCRT-0 and polyubiquitin condensates create high-density cargo sorting sites on vacuolar membrane. Model suggesting how variation of ESCRT and cargo density affects recruitment and condensation of early ESCRT and substrate on the surface

of membranes. The condensation of early players in the pathway may nucleate downstream assembly, leading to ESCRT-III polymerization and membrane budding. At sites of lower-density ESCRT-binding modules (such as the vacuolar membrane in yeast), polyubiquitin-mediated condensation would be more critical for cargo sorting organization, compared to endosomes, with an already existing high-density of ESCRT.

Movie 1: *In vivo* visualization of Ypq1-GFP-2X-FKBP upon addition of rapamycin. Yeast cells were treated with 1 µg/mL of Rapamycin and imaged over the timeframe indicated in the movie.

Movie 2: Fusion of ESCRT-0 and 4X-Ubiquitin membrane clusters. Purified Vps27, Hse1, His6-Ub4X-Cy5 were added to supported bilayers and imaged every 30 s after about 5-10 minutes.

Movie 3: Fusion of ESCRT-0 and 4X-Ubiquitin 3D droplets. Droplets of Vps27, Hse1 and His6-Ub4X-Cy5 were allowed to form (~30 minutes), and time-lapse images were acquired on a confocal microscope.

Supplementary Materials:

Figure S1

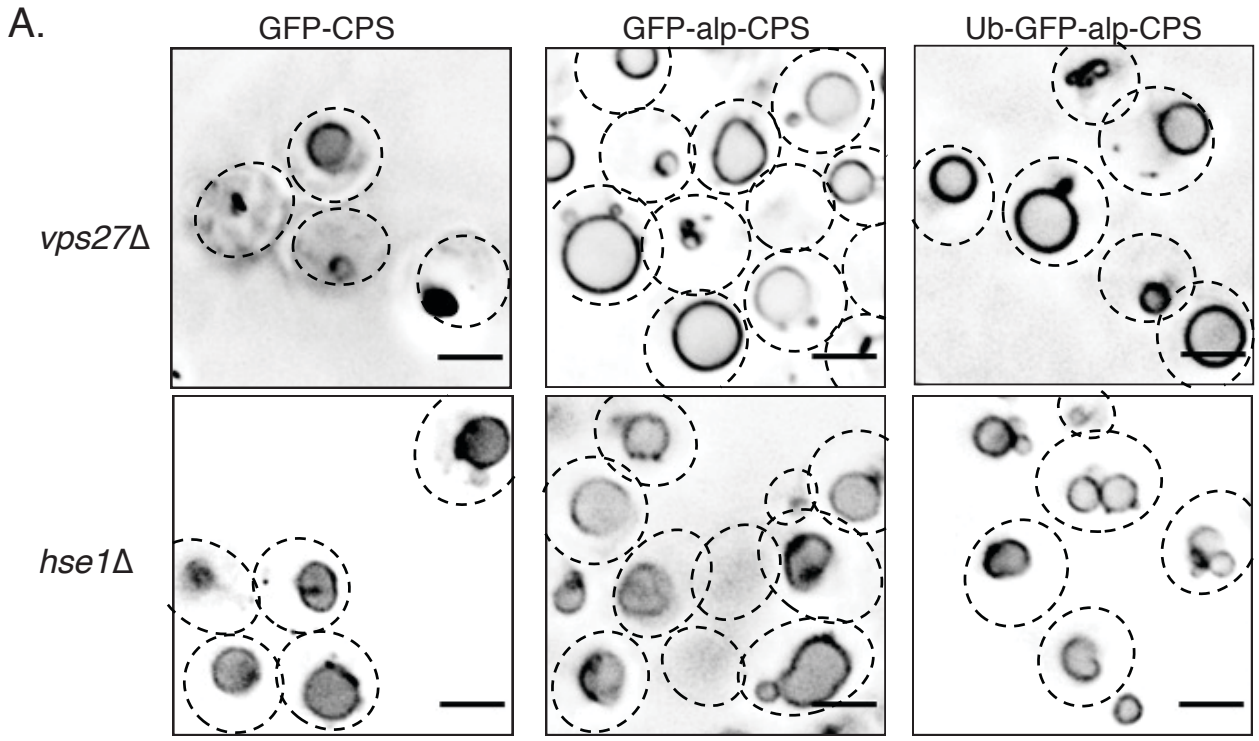

735

Fig. S1. Localization of endosomal and vacuolar GFP-CPS molecules. B) Localization of different GFP-CPS constructs in the ESCRT-0 components *vps27*Δ and *hse1*Δ strains. Scale bars are 2 µm each.

Figure S2

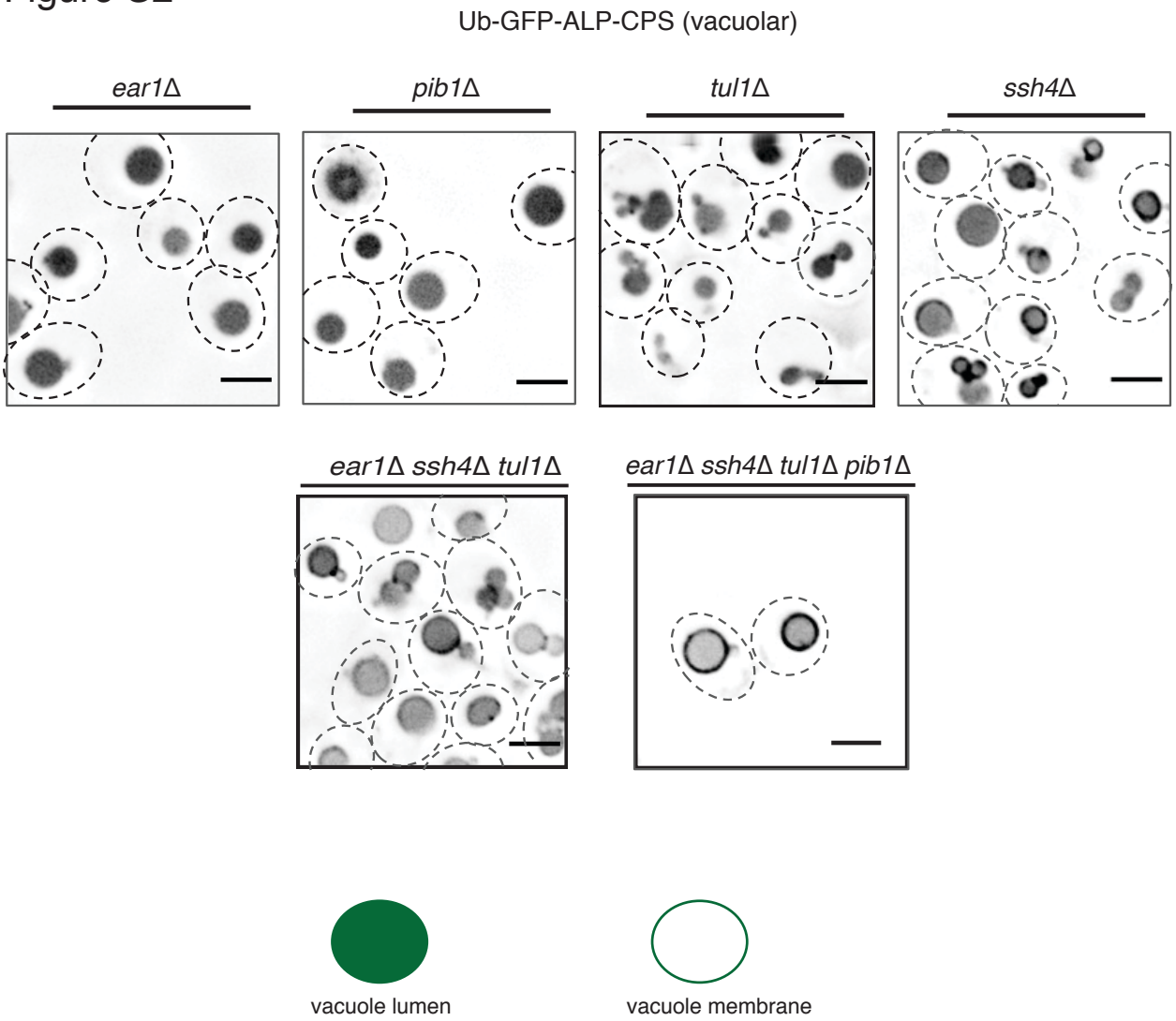

740

Fig. S2. **Poly-ubiquitination is critical for vacuolar sorting of ESCRT cargo.** Localization of Ub-GFP-alp-CPS (ubiquitin conjugated vacuolar cargo) in the *ear1*Δ *ssh4*Δ *pib1*Δ *tul1*Δ or the individual strains. Scale bars are 2 µm each.

Figure S3

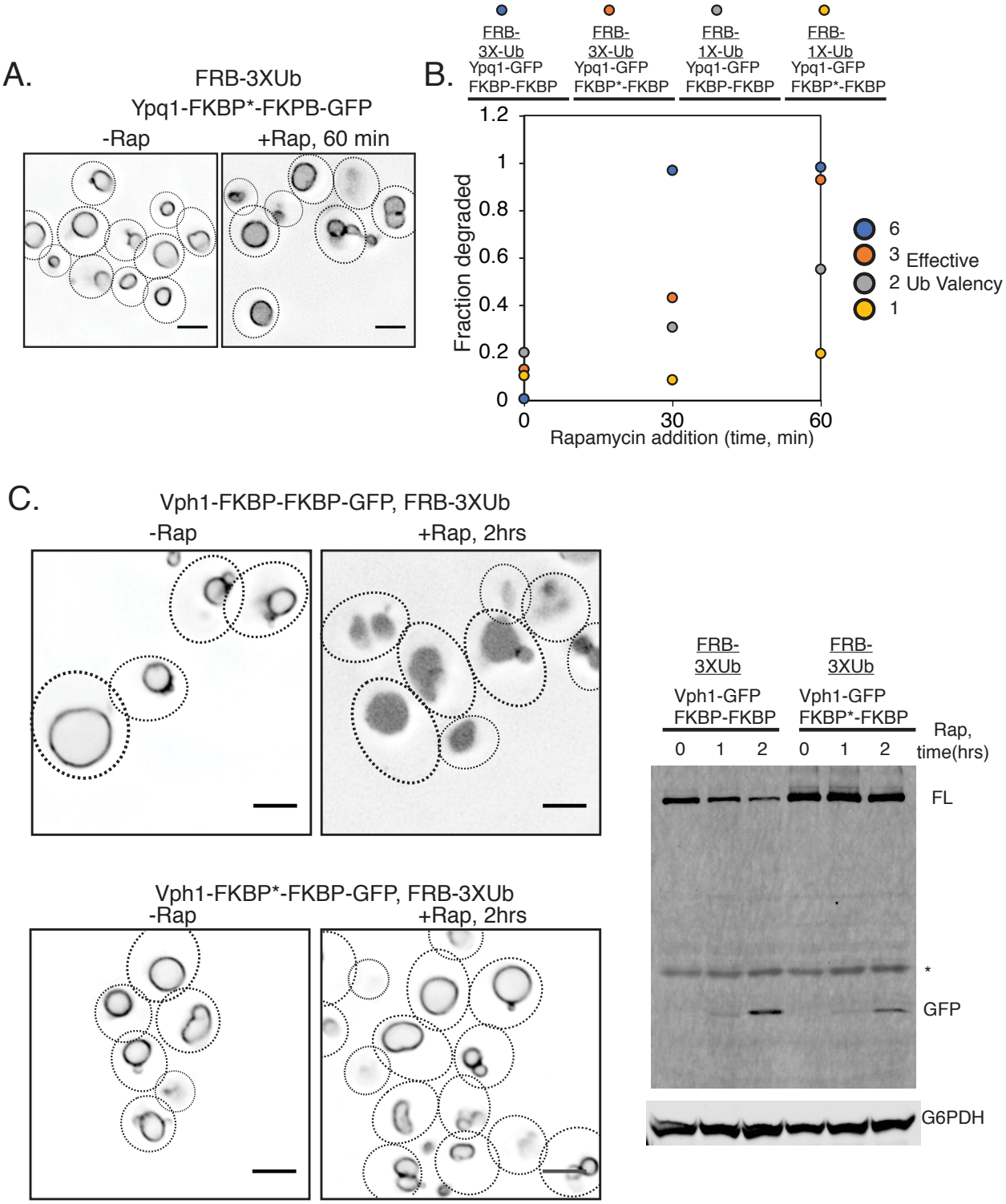

745

Fig. S3. Multivalent interactions of polyubiquitin and ESCRT-0 promotes cargo sorting. A) Effect of rapamycin-induced sorting of Ypq1 construct with one FKBP site mutated and can no longer interact with FRB. Strain consists of FRB-3X ubiquitin and the imaging was done before

adding rapamycin and after 60 minutes of adding rapamycin. **B)** Kinetics of different Ypq1-GFP-FKBP molecules in the presence of different FRB-Ub molecules. Colors of circles indicate the effective valency of ubiquitin achieved from the combination of FKBP and FRB constructs. **C)** Vph1-GFP-FKBP-FKBP constructs sorting in the presence of FRB-3XUb. Mutation in one of the FRB binding sites in FKBP inhibits sorting of the Vph1 construct, signifying the effect of multivalent interactions in sorting efficiency. Left figures are imaging experiments following GFP-tagged Vph1, and the right image is an immunoblot following GFP cleavage after adding rapamycin for the indicated times.

Figure S4

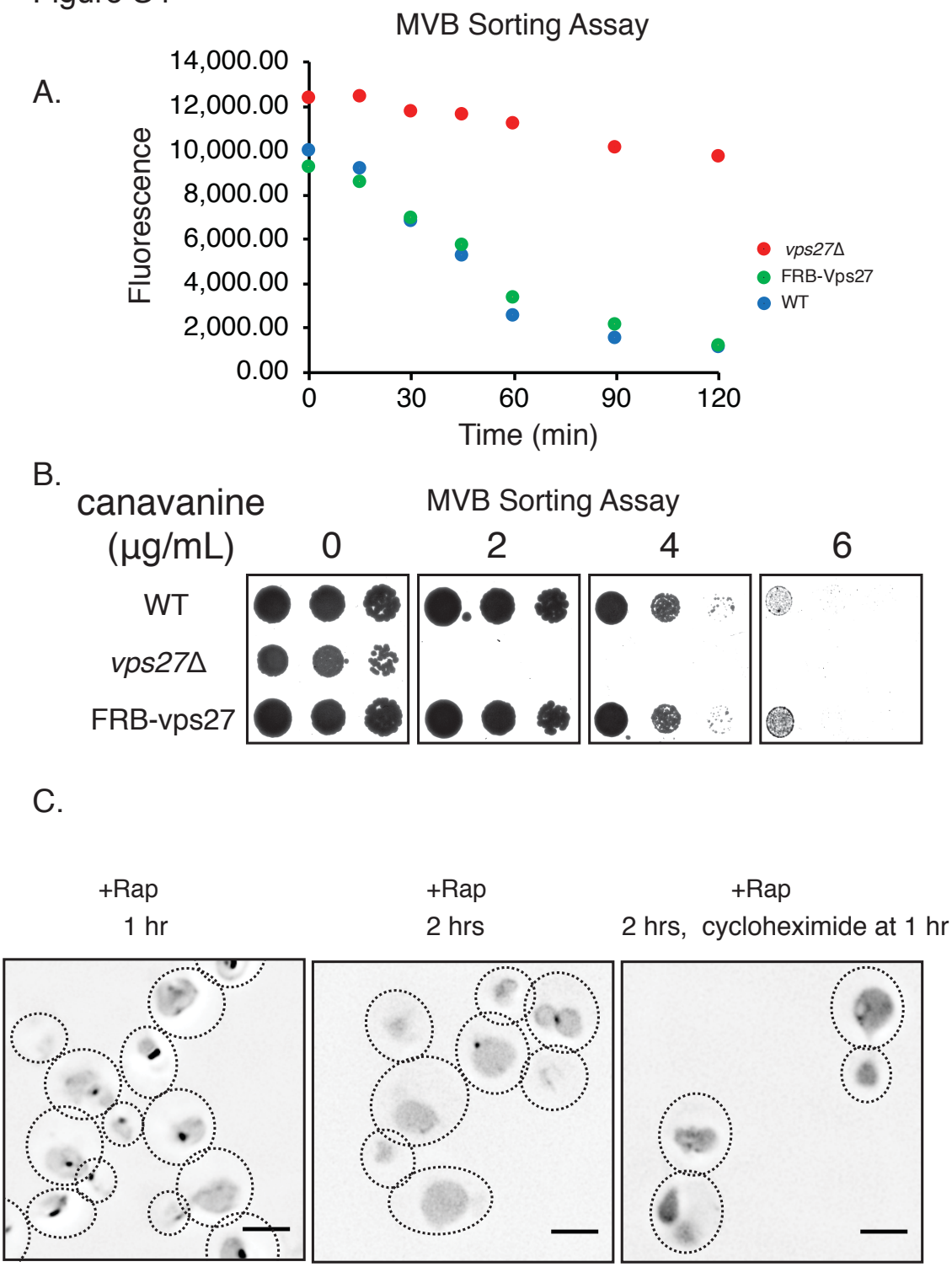

Fig. S4. Recruitment of ESCRT-0 to vacuolar membrane induces cargo clustering. A-B) FRB-Vps27 construct used is identical to WT Vps27 in cargo sorting assays for the cargoes Mup1 in Mup1-pHluorin sorting **(A)** and Can1 sorting canavanine assays **(B)**. **C)** With time or with

translation inhibition, the clusters induced by FRB-Vps27 recruitment disappear, presumably by internalization into the vacuolar lumen.

Figure S5

A.

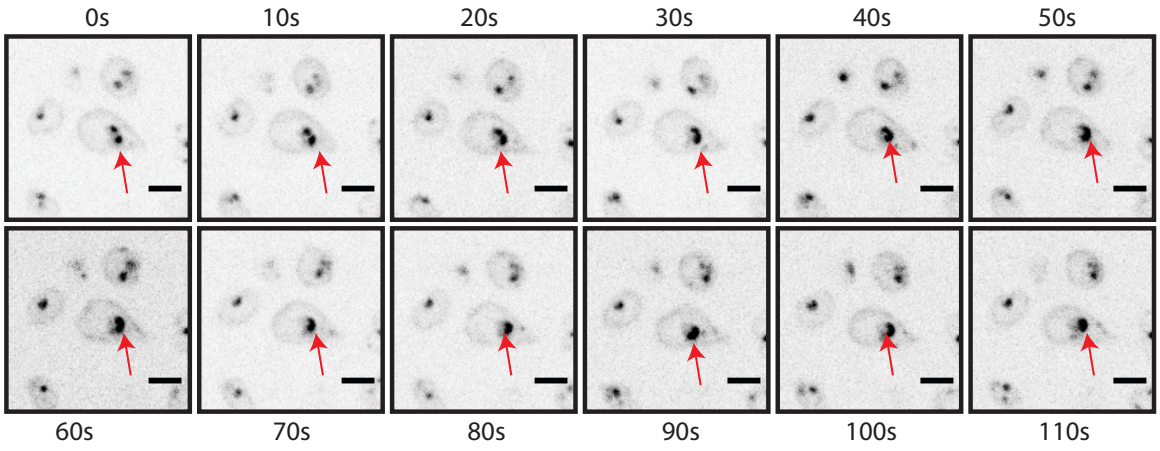

B.

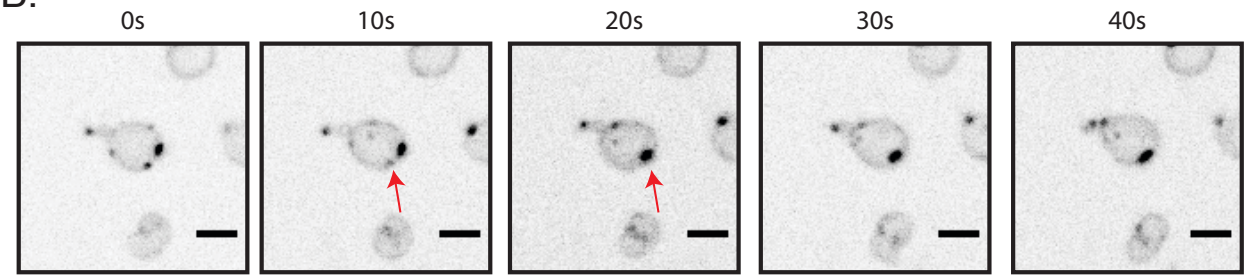

C.

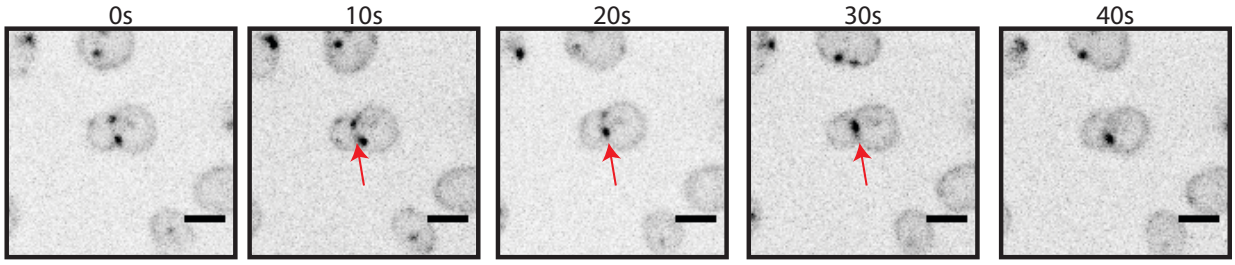

765 **Fig. S5. *In vivo* dynamics of clusters of Ypq1-GFP-2XFKBP molecule induced by recruitment of FRB-Vps27 (A-C).** In these experiments, rapamycin was added for 30 minutes the imaging was performed with 10 ms interval. Scale bars are 2 μm each.

Figure S6

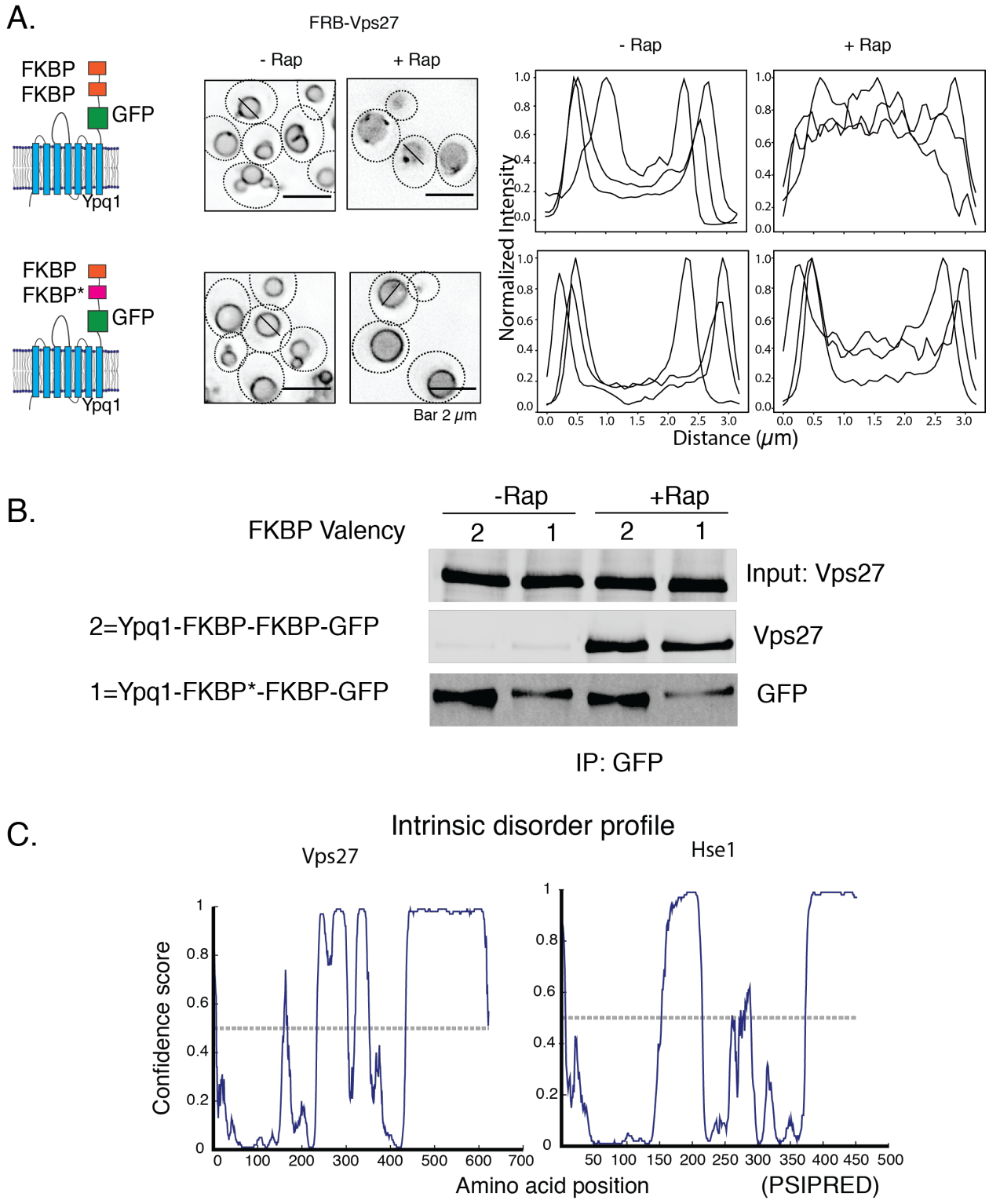

Fig. S6. Valency effect on ESCRT-0 recruitment and cargo sorting. A) Ypq1-GFP-FKBP-FKBP or one of the FKBPs mutated to abrogate FRB binding were imaged after adding rapamycin

770 to strains consisting of FRB-Vps27. Cargo clustering and internalization are reduced in the strain expressing the lower valency molecule. Graphs on the right are representative normalized intensity profiles of line-scans across vacuoles from microscopy images. **B)** Immunoprecipitation of GFP in Ypq1-GFP-FKBP-FKBP and FRB-Vps27 expressing strains and blotting for Vps27. FRB-Vps27 is still bound to Yqp1-GFP-FKBP*-FKBP in a rapamycin dependent fashion. **C)** Intrinsic-
775 disorder profile obtained from DISOPRED for the ESCRT-0 components Vps27 and Hse1.

Figure S7

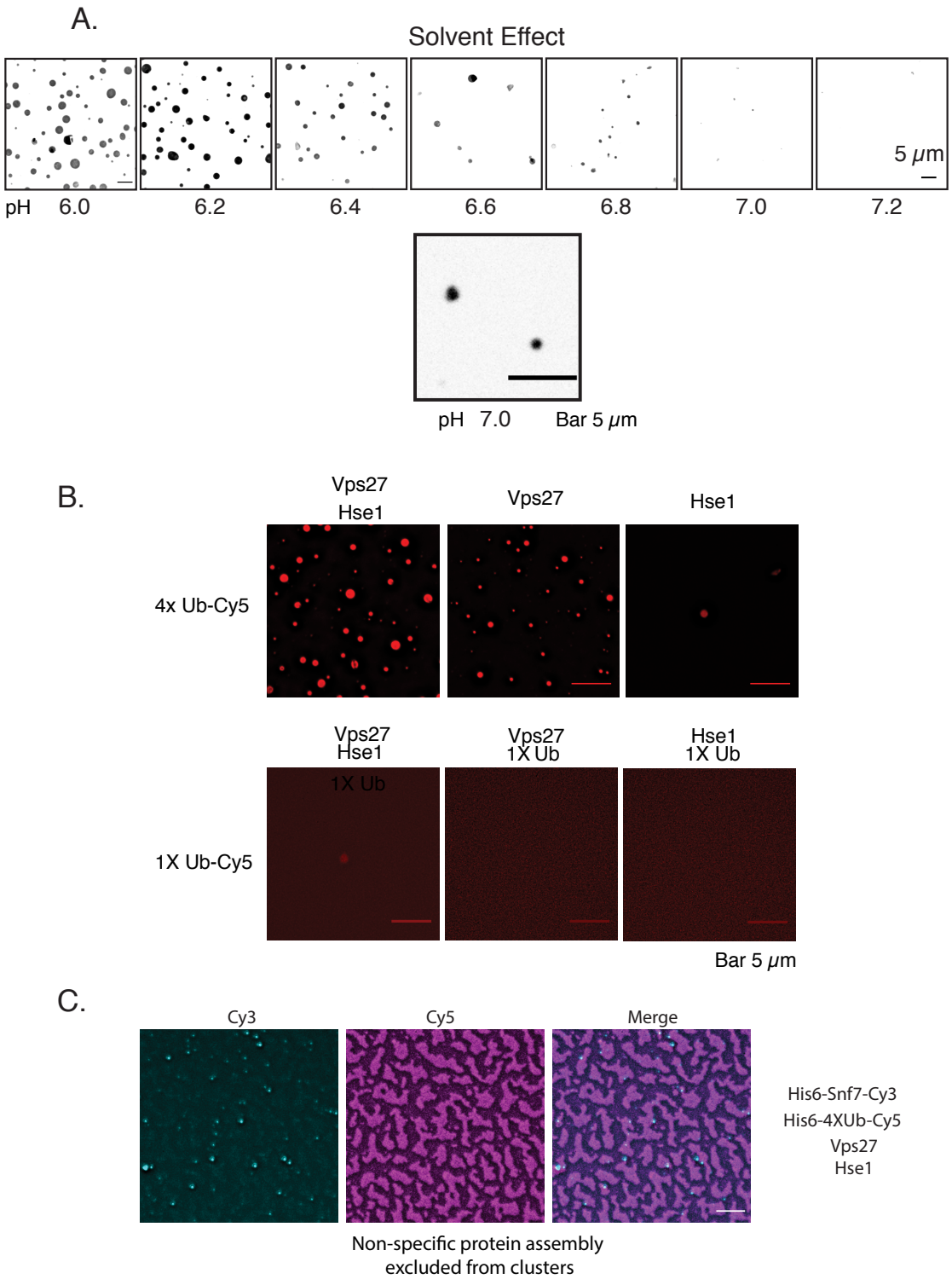

Fig. S7. Condensation of ESCRT-0 and polyubiquitin assemblies. A) Solvent effect on the condensation of ESCRT-0 and 4X ubiquitin. pH was varied by using different buffers of Bis-Tris at the indicated pH values. Concentration of buffer was kept at 100 mM and NaCl was kept

constant at 150 mM. Images were taken after two hours of assembling the components at room temperature. Bottom figure shows a zoomed-in image of the droplets at pH 7, showing presence of droplets but at reduced numbers. Scale bars are 5 µm each. **B)** Assemblies of ESCRT-0 and either 4XUb or 1X Ub at the indicated compositions (either both ESCRT-0 components or singles, as represented on the top of the panels). Concentrations of the molecules were at 5 µM, and the buffer was 25 mM Bis Tris pH 6.5, 150 mM NaCl. **C**) 100 nM His6-Snf7-Cy3 forms punctate structures that are excluded from ESCRT-0 (500 nM Vps27 and 500 nM Hse1), 500 nM 4X -Ubiquitin (Cy5) clusters. Experiment was performed in 25 mM Bis Tris pH 6.5, 150 mM NaCl, with imaging performed after 1 hour of protein incubation on the membrane.

Figure S8

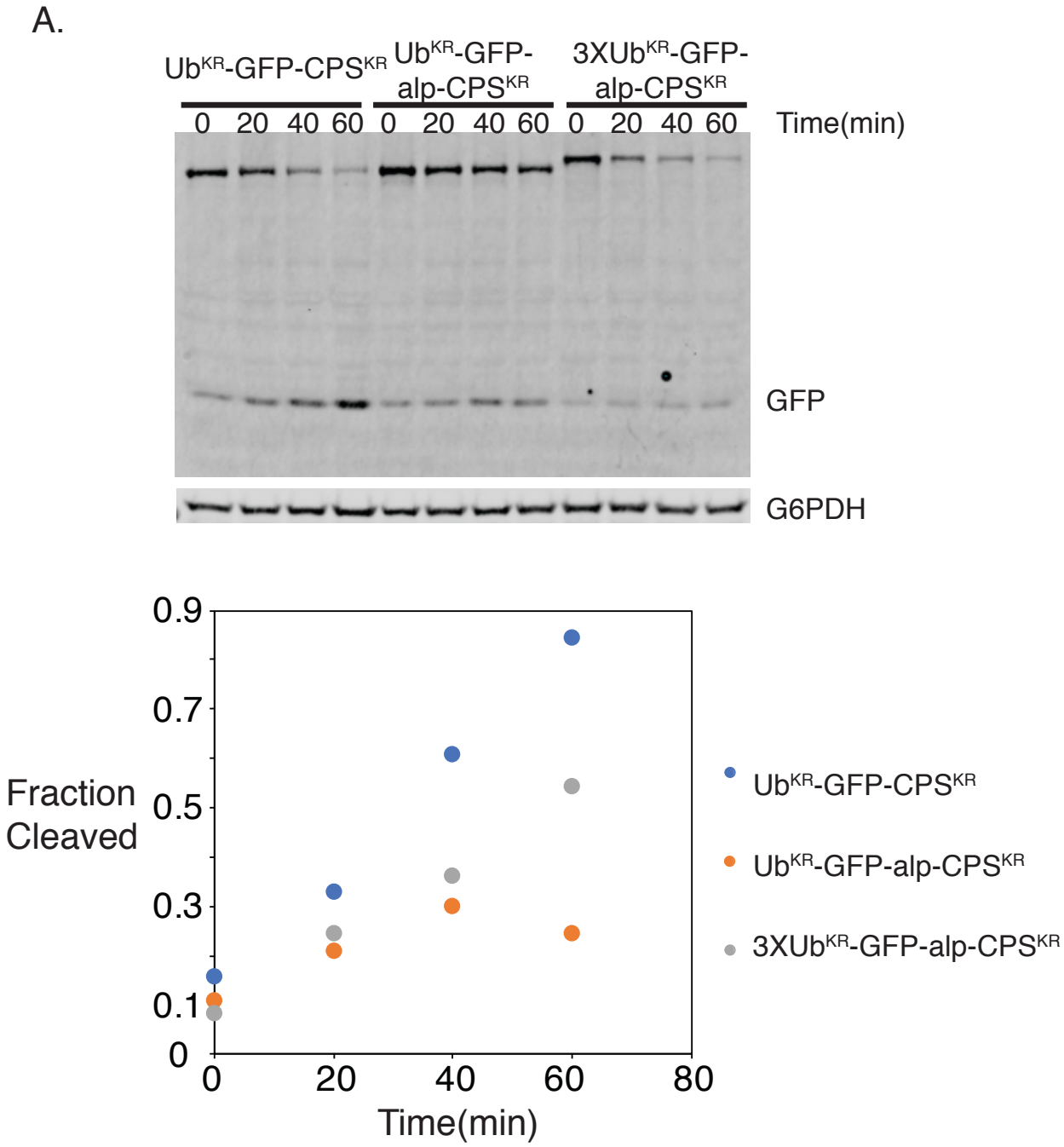

Fig. S8. Enhancing ubiquitin chain length induces vacuolar cargo sorting. A) Kinetics of the degradation of Ub^{KR}-GFP-CPS (endosomal), Ub^{KR}-GFP-alp-CPS (vacuolar), or $3XUb^{KR}$-GFP-alp-CPS proteins upon induction of expression for 20 minutes and further inhibition of translation with cycloheximide addition. The 0 timepoint represents 20 minutes of GAL induction with no cyloheximide. **B)** Graphical representation of the fraction degraded, with data from **A)**.

Figure S9

A.

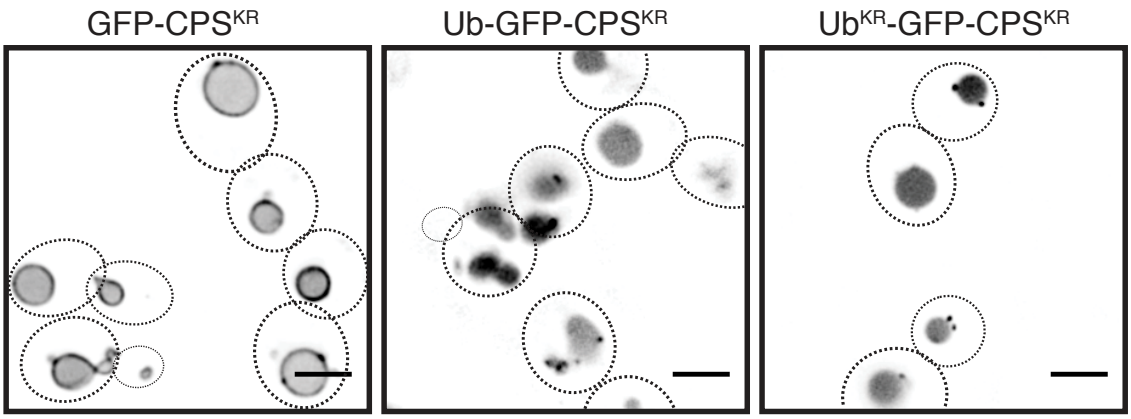

Endosomal (no alp motif)

B.

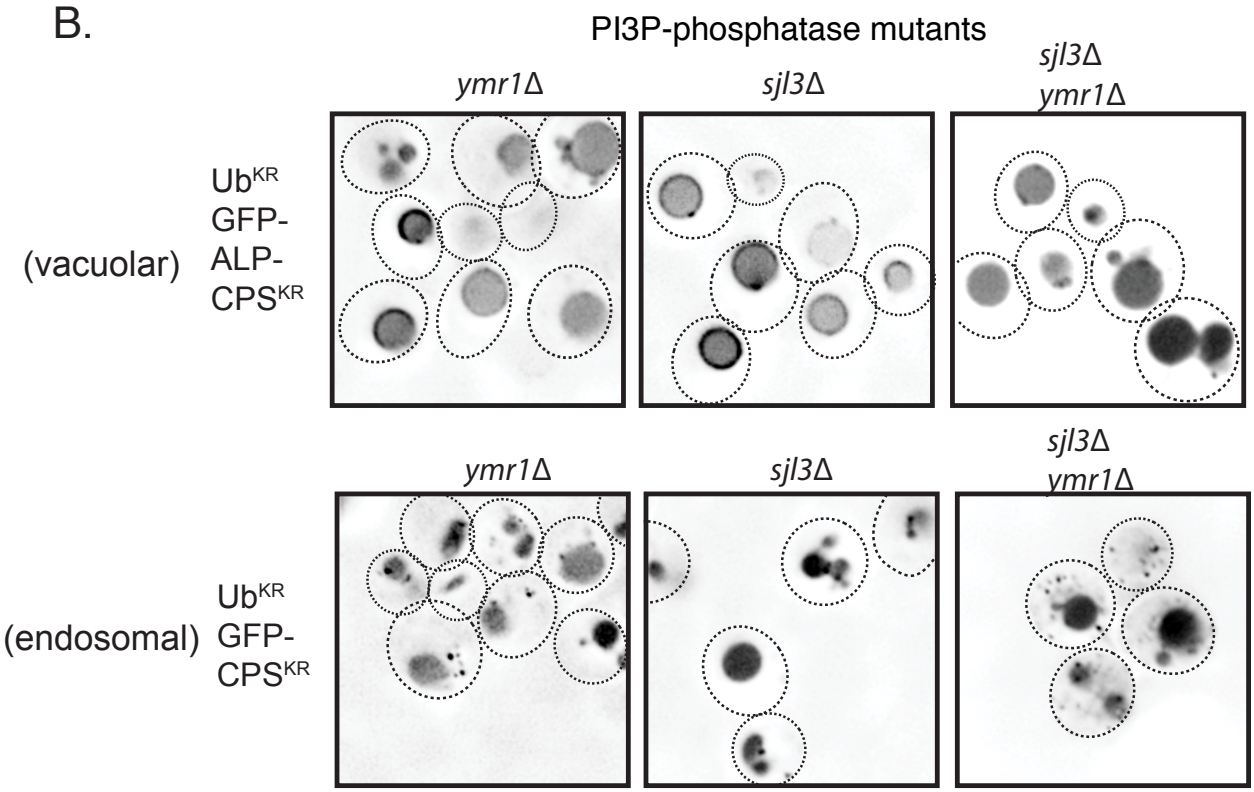

Fig. S9. **A)** Localization of the GFP-CPS constructs with the K8R K12R (KR) mutations, when conjugated with ubiquitin or Ub^{KR}. Ub^{KR} has all the lysines mutated to Arg. CPS^{KR} represents two mutations: K8R and K12R in the cytosolic region of CPS. B) Localization of the different CPS constructs in the phosphatase mutants *ymr1*Δ and *sjl3*Δ.

Figure S10

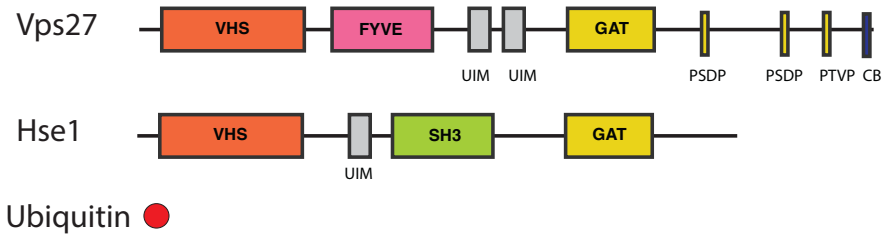

ESCRT-0 heterodimers and homodimers

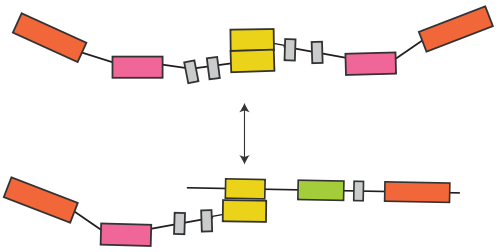

Weak self-assembly between
ESCRT-0 heterodimers

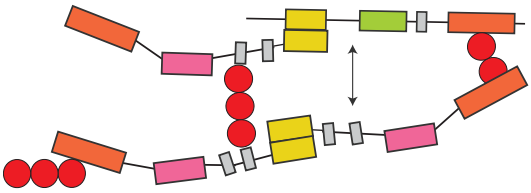

Enhanced self-assembly
due to close proximity

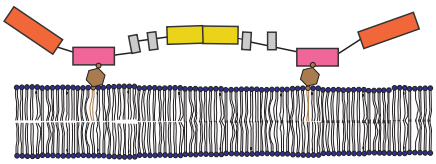

Higher density of PI3P enhance association
rates of ESCRT-0 molecules, increasing propensity
to self-assemble

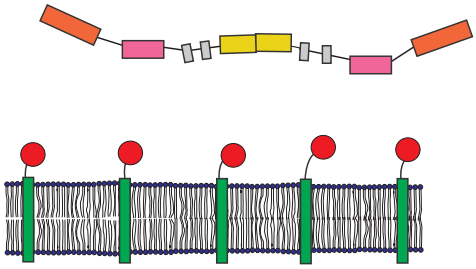

ESCRT-0 in solution,
no self-association with no PI3P
on membrane and mono-ubiquitinated cargo

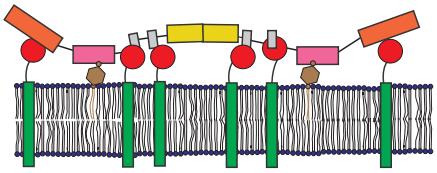

Recruitment and concentrated on 2D surface,
leading to enhanced self association
and cargo clustering

805 **Fig. S10. ESCRT-0 and ubiquitin assembly models on the surface of membranes.** Surface density as regulated by lipid species, multivalency through polyubiquitin and multiple ubiquitin binding sites, and self-assembly through homo and hetero-oligomerization synergize to affect cargo condensation on membranes.

810

Table 1: Strains and Plasmids

Designation in Manuscript	Source or reference	Other names	Additional information	Additional Notes
WT	PMID:3062374	SEY6210	*(background strain) MATα ura3-52 his3-200 leu2-3,112 trp1-901 lys2-801 suc2-9*	
WT	PMID:3062374	SEY6210.1	*(background strain) MATa leu2-3,112 ura3-52 his3-Δ200 trp1-Δ901 lys2-801 suc2-Δ9*	
WT; *Mup-pHluorin*	PMID: 24139821	NBY40	*(SEY6210.1); MUP1-pHLUORIN::KANMX*	
GFP-CPS	This study	SBY309	*SEY6210; GFP-CPS::URA3*	
GFP-ALP-CPS	This study	SBY301	*SEY6210; GFP-ALP-CPS::URA3*	
Ub^{KR}GFP-alp-CPS	This study	SBY318	*SEY6210; K0UbGFP-alp-CPSK8RK12R::URA3*	All Ub lysines mutated to argininines, K8R and K12R in CPS
2XUb^{KR}GFP-alp-CPS	This study	SBY399	*SEY6210; 2XUbK0-GFP-alp-CPSK8RK12R::URA3*	All Ub lysines mutated to argininines, K8R and K12R in CPS
3XUb^{KR}GFP-alp-CPS	This study	SBY398	*SEY6210;3XUbK0-GFP-alp-CPSK8RK12R::URA3*	All Ub lysines mutated to argininines, K8R and K12R in CPS
doa4Δ pep4Δ prb1Δ; UB-GFP-alp-CPS	This study	SBY470	*SEY6210;doa4Δ::LEU2 pep4Δ::HIS3 prb1Δ::KAN ;Ub- GFP-alp-CPS::URA3*	
doa4Δ pep4Δ prb1Δ; UB^{KR}-GFP-alp-CPS	This study	SBY469	*SEY6210;doa4Δ::LEU2 pep4Δ::HIS3 prb1Δ::KAN ;Ub(K0)- GFP-alp-CPSK8RK12R::URA3*	All Ub lysines mutated to argininines, K8R and K12R in CPS
Ub-GFP-alp-CPS	This study	SBY264	*SEY6210;UB-GFP-alp-CPS::URA3*	
Ypq1-GFP-FKBP-FKBP; FRB-3XUb	This study (modified from PMID: 28661397)	SBY124	*SEY6210.1, tor1-1, MATa, fpr1Δ::NAT, YPQ1-GFP 2XFKBP::TRP; 305-FRB-HA-3XUb(GE)::Leu2*	Rapamycin resistant mutants (*tor1-1*, *fpr1Δ*, C-terminal glycine in Ub mutated to Glu)
Ypq1-GFP-FKBP-FKBP; FRB-1XUb	This study	SBY126	*SEY6210.1, tor1-1, MATa, fpr1Δ::NAT, YPQ1-GFP 2XFKBP::TRP; 305-FRB-HA-1XUb(GE)::Leu2*	Rapamycin resistant mutants (*tor1-1*, *fpr1Δ*, C-terminal glycine in Ub mutated to Glu)
Ypq1-GFP-FKBP-FKBP; FRB-3XUb*	This study	SBY238	*SEY6210.1, tor1-1, MATa, fpr1Δ::NAT, YPQ1-GFP-FKBP*-FKBP::TRP; 305-FRB-HA-3XUb(GE)::Leu2; Vph1-mcherry::KAN*	Rapamycin resistant mutants (*tor1-1*, *fpr1Δ*, C-terminal glycine in Ub mutated to Glu), FKBP* here is a three-site mutation (see Materials and Methods) for sequence
Ypq1-GFP-FKBP-FKBP; FRB-1XUb*	This study	SBY408	*SEY6210.1, tor1-1, MATa, fpr1Δ::NAT, YPQ1-GFP-FKBP*-FKBP::TRP; 305-FRB-HA-1XUb(GE)::Leu2*	Rapamycin resistant mutants (*tor1-1*, *fpr1Δ*, C-terminal glycine in Ub mutated to Glu), FKBP* here is a three-site mutation (see Materials and Methods) for sequence
Ypq1-GFP-FKBP-FKBP; FRB-Vps27	This study	SBY204	*SEY6210.1, tor1-1, MATa, fpr1Δ::NAT, YPQ1-GFP-2XFKBP::TRP; 305-FRB-Vps27::Leu2*	
Ypq1-GFP-FKBP-FKBP; FRB-Vps27*	This study	SBY409	*SEY6210.1, tor1-1, MATa, fpr1Δ::NAT, YPQ1-GFP-FKBP*-FKBP::TRP; 305-FRB-Vps27::Leu2*	
vps27Δ hse1Δ; Mup-pHluorin	PMID: 27074665	STY41	*SEY6210; vps27Δ::HIS3; hse1Δ::HIS3; Mup1-pHluorin::KAN*	
VPS27 hse1Δ ; Mup-pHluorin	This study	SBY517	*SEY6210; vps27Δ::HIS3; hse1Δ::HIS3; Mup1-pHluorin::KAN; VPS27::URA3*	
vps27 uim uim ; Mup-pHluorin	This study	SBY519	*SEY6210; vps27Δ::HIS3; hse1Δ::HIS3; Mup1-pHluorin::KAN; vps27 S270D S313D:: URA3*	
vps27 vhs ; Mup-pHluorin	This study	SBY520	*SEY6210; vps27Δ::HIS3; hse1Δ::HIS3; Mup1-pHluorin::KAN; vps27 L28D L32D:: URA3*	
vps27 vhs uim uim ; Mup-pHluorin	This study	SBY521	*SEY6210; vps27Δ::HIS3; hse1Δ::HIS3; Mup1-pHluorin::KAN; vps27 L28D L32D S270D S313D:: URA3*	
pGAL Ub^{KR} GFP alp CPS; GEV; vph1-mcherry	This study	SBY432	*SEY6210; vph1-mcherry::TRP; 305-GEV::Leu2; 306-(gal)- K0Ub GFPalpCPSK8RK12R::URA3*	

pGAL Ub^{KR} GFP CPS; GEV; vph1-mcherry	This study	SBY433	*SEY6210; vph1-mcherry::TRP; 305-GEV::Leu2; 306-(gal)-K0Ub GFPCPSK8RK12R::URA3*	
sjl3Δ ; Ub^{KR} GFP alp CPS	This study	SBY461	*SEY6210.1;sjl3Δ::TRP1; 306-UbK0-GFP-alp-CPS-K8R K12R::URA3*	
ymr1Δ ; Ub^{KR} GFP alp CPS	This study	SBY458	*SEY6210.1;ymr1Δ::HIS3+306-UbK0scge-GFP-alp-CPS-K8R K12R::URA3*	
sjl3Δ ymr1Δ ; Ub^{KR} GFP alp CPS	This study	SBY456	*SEY6210.1; ymr1Δ::HIS3, sjl3Δ::TRP1; 306-UbK0-GFP-alp-CPS-K8R K12R:: URA3*	
sjl3Δ ; Ub^{KR} GFP CPS	This study	SBY460	*SEY6210.1;sjl3Δ::TRP1; 306-K0Ub-GFP-CPSK8RK12R::URA3*	
ymr1Δ ; Ub^{KR} GFP CPS	This study	SBY459	*SEY6210.1;ymr1Δ::HIS3;306-K0Ub-GFP-CPSK8RK12R:URA3*	
sjl3Δ ymr1Δ ; Ub^{KR} GFP CPS	This study	SBY457	*SEY6210.1; ymr1Δ::HIS3, sjl3Δ::TRP1; 306-UbK0-GFP-CPS-K8R K12R:: URA3*	
sjl3Δ ymr1Δ	PMID: 15169871	BPY01	*SEY6210.1; ymr1Δ::HIS3, sjl3Δ::TRP1*	
GFP-CPS; vph1-mcherry	This study	SBY483	*SEY6210; 306-(cps1p)-GFP-CPS::URA3; Vph1mcherry::KAN*	
GFP-alp-CPS; vph1-mcherry	This study	SBY513	*SEY6210; 306-(cps1p)-GFP-alp-CPS::URA3; Vph1-mcherry::KAN*	
vps27Δ; GFP-CPS	This study	SBY314	*vps27Δ:HIS3; 306-(cps1p)-GFP-CPS::URA3*	
vps27Δ; GFP-alp-CPS	This study	SBY315	*vps27Δ:HIS3; 306-(cps1p)-GFP-alp-CPS::URA3*	
vps27Δ; Ub-GFP-alp-CPS	This study	SBY375	*vps27Δ:HIS3; 306-(cps1p)-Ub-GFP-alp-CPS::URA3*	
hse1Δ; GFP-CPS	This study	SBY331	*hse1Δ::HIS3; 306-(cps1p)-GFP-CPS::URA3*	
hse1Δ; GFP-alp-CPS	This study	SBY332	*hse1Δ::HIS3; 306-(cps1p)-GFP-alp-CPS::URA3*	
hse1Δ; Ub-GFP-alp-CPS	This study	SBY334	*hse1Δ::HIS3; 306-(cps1p)-Ub-GFP-alp-CPS::URA3*	
tul1Δ; Ub-GFP-alp-CPS	This study	SBY284	*SEY6201.1;tul1Δ::HIS3; Ub-GFP-alp-CPS::URA3*	
ssh4Δ; Ub-GFP-alp-CPS	This study	SBY296	*SEY6201.1;ssh4Δ::TRP1; Ub-GFP-alp-CPS::URA3*	
ear1Δ; ssh4Δ; tul1Δ; Ub-GFP-alp-CPS	This study	SBY452	*6210, ear1Δ::NAT, ssh4Δ::KAN, tul1Δ::TRP; Ub-GFP-alp-CPS::URA3*	
ear1Δ; ssh4Δ; tul1Δ; pib1Δ; Ub-GFP-alp-CPS	This study	SBY453	*6210, ear1Δ:: NAT, ssh4Δ::KAN, tul1Δ::TRP, pib1Δ::HPH; Ub-GFP-alp-CPS::URA3*	
Vph1-GFP-FKBP-FKBP; FRB-3XUb	PMID: 28661397	LZY560	*SEY6201.1; tor1-1, MATa, fpr1Δ::NAT, VPH1-GFP 2XFKBP::TRP1; FRB-3XUb(ge)::leu2*	Rapamycin resistant mutants (*tor1-1*, *fpr1Δ*, C-terminal glycine in Ub mutated to Glu)
Vph1-GFP-FKBP-FKBP; FRB-3XUb*	This study	SBY215	*SEY6201.1; tor1-1, MATa, fpr1Δ::NAT, VPH1-GFP-FKBP*-FKBP::TRP1; FRB-3XUb(ge)::leu2*	Rapamycin resistant mutants (*tor1-1*, *fpr1Δ*, C-terminal glycine in Ub mutated to Glu), FKBP* here is D37V W59A
vps27 Δ Mup1-pHluorin	PMID: 27074665	STY30	*SEY6210; vps27Δ::HIS3; Mup1-pHluorin::KAN*	
pGAL 3X Ub^{KR} GFP alp CPS; GEV	This study	SBY426	*SEY6210; 305-GEV::Leu2; 306-(gal)- 3X-K0Ub GFPalpCPSK8RK12R::URA3*	
GFP - CPS ^{KR}	This study	SBY363	*SEY6210; 306-GFP-CPS K8R K12R::URA3*	
Ub-GFP-CPS ^{KR}	This study	SBY307	*SEY6210; 306-(cps1p)-UbscgeGFPCPSK8RK12R:URA3*	
Ub^{KR}-GFP-CPS^{KR}	This study	SBY365	*SEY6210; 306-UbK0-GFPCPSK8RK12R::URA3*	
GAL ESCRT-0 Complex	This study	SBY197	*SEY6210 ADH1pro-GAL4BD-hER-VP16(GEV):TRP; pRS306-GFPHse1-GAL-Vps27::URA3*	

Vector	PMID: 2659436	pRS416		
Vector	PMID: 2659436	pRS414		
Vector	PMID: 2659436	pRS415		
Vps27	This study	pET28aH6SUMOVps27tevS		
Hse1	This study	pET28aH6SUMOHse1tevS		
His6Ub4X	This study	pET28aH6SUMO-His6-cys-4XUb		
His6Ub1X	This study	pET28aH6SUMO-His6-cys-1XUb		
His6Snf7	This study	pET23d(+)H6Snf7C241	*c-terminal cysteine appended to Snf7*	
Vps27-*vhsuimuim*	This study	pET28aH6SUMOVps27*vhsuimuim tevS*	*Vps27 L28D L32D S270D S313D*	
ESCRT-0 complex	This study	pRS306 - GAL GFP-Hse1;GAL Vps27		
Hse1 vhs	This study	pRS415 Hse1 W25A		
Hse1 vhs uim	This study	pRS415 Hse1 W25A S172D		
Hse1 uim	This study	pRS415 Hse1 S172D		
Vps27	This study	pRS416 Vps27		
Hse1	This study	pRS415 Hse1		